Compressive Stress Enhances Invasive Phenotype of Breast Cancer Cells via Piezo1 Activation

Mingzhi Luo
Changzhou University
Kenneth KY Ho
University of Michigan
Zhaowen Tong
University of Michigan
Linhong Deng
Changzhou University
Allen Liu (allenliu@umich.edu)
University of Michigan https://orcid.org/0000-0002-0309-7018

Research article

Keywords: Compressive stress, Piezo1, caveolae, invadopodia, mechanotransduction

Posted Date: December 6th, 2019

DOI: https://doi.org/10.21203/rs.2.18102/v1

Compressive Stress Enhances Invasive Phenotype of Breast Cancer Cells via Piezo1 Activation

Mingzhi Luo[1,2], Kenneth K. Y. Ho[1], Zhaowen Tong[3], Linhong Deng[2,*], Allen P. Liu[1,3,4,5,*]

[1] Department of Mechanical Engineering, University of Michigan, Ann Arbor, Michigan, United States

[2] Institute of Biomedical Engineering and Health Sciences, Changzhou University, Changzhou, Jiangsu, P. R. China

[3] Department of Biophysics, University of Michigan, Ann Arbor, Michigan, United States

[4] Department of Biomedical Engineering, University of Michigan, Ann Arbor, Michigan, United States

[5] Cellular and Molecular Biology Program, University of Michigan, Ann Arbor, Michigan, United States

* Corresponding author: Linhong Deng, +86-13685207009, dlh@cczu.edu.cn; Allen P. Liu, +1-734-764-7719, allenliu@umich.edu

Running title: Compression promotes invasion *via* Piezo1

Keywords: Compressive stress, Piezo1, caveolae, invadopodia, mechanotransduction

Abstract

Uncontrolled growth in solid tumor generates compressive stress that drives cancer cells into invasive phenotypes, but little is known about how such stress affects the invasion and matrix degradation of cancer cells and the underlying mechanisms. Here we show that compressive stress enhanced invasion and matrix degradation of breast cancer cells. We further identified Piezo1 as the putative mechanosensitive cellular component that transmits compressive stress to induce calcium influx, which in turn activate Src/ERK signaling. Interestingly, we observed actin protrusions with matrix degradation ability on the apical side of the cells. Furthermore, we demonstrate that Piezo1 channels were partially localized in caveolae, and reduction of caveolin-1 expression or disruption of caveolae with methyl-β-cyclodextrin led to not only reduced Piezo1 expression but also attenuation of the invasive phenotypes promoted by compressive stress. Taken together, our data indicate that mechanical compressive stress activates Piezo1 channels to mediate enhanced cancer cell invasion and matrix degradation that may be a critical mechanotransduction pathway during, and potentially a novel therapeutic target for, breast cancer metastasis.

Introduction

Cancer invasion is a cumulative result of multiple processes including directed cell migration and extracellular matrix (ECM) degradation. While biochemical factors are well known in mediating cancer invasion, mechanical forces such as compressive stress have also been identified as essential regulators of these processes[1]. For example, an increase of compressive stress inside solid tumor accompanies with cell proliferation and stiffness enhancement[2]. Cancer cells also experience compressive stress when they migrate through capillary and confined tissue microenvironment[3,4]. Recent *in vivo* studies show that compressive stress stimulates tumorigenic signaling in colon epithelial cells[5], and strategies to release compressive stress can indeed enhance the efficiency of anti-tumor treatment[6]. Interestingly, it is demonstrated *in vitro* that compressive stress directly alters cancer cell proliferation and migration[7,8] and thus drives them to invasive phenotypes[9]. However, whether compressive stress enhances invasive phenotypes by promoting matrix degradation of cancer cells and how compressive stress is sensed and transduced into cellular behaviors is still poorly understood.

Considering that compressive stress stretches cell membrane and thus increases membrane tension, it may alter cancer cells' behaviors through tension-mediated conformational changes of proteins and lipids in the membrane[10]. In particular, the increase of membrane tension can activate several stretch-activated ion channels (SAC) including Piezo and transient receptor potential (TRP) channels[11-14]. Comparing to TRP channels, Piezo channels are known to respond to membrane tension with more exquisite sensitivity[15,16], and can be activated via cytoskeleton-mediated forces [17,18]. Moreover, studies *in vivo* show that Piezo channels mediate diverse physiological activities that are associated with compressive stimulation including touch perception[11] and blood pressure sensing[19], and are essential in some mechanically related pathological processes such as breast cancer development[20]. In the case of breast cancer development, the role of Piezo1 is substantiated by the shorter survival times of patients with upregulated Piezo1 mRNA expression level[20]. More importantly, it has been shown that the breast cancer cells' response to compression is dependent on

Piezo but not TRP channels[21]. Upon the activation of Piezo1 channels, calcium influx evokes several downstream signaling pathways such as Src and ERK which in turn affect dynamics of actin-based structures such as invadopodia/invadosomes[22] that degrade extracellular matrix proteins and thus promote invasion[23]. These data indicate that Piezo1 may be essential for the compression-enhanced cancer invasion. However, whether and how Piezo1 channels mediate compression-enhanced invasive phenotype of cancer cells has not been examined.

So far it is generally known that SAC functions at “membrane force foci” such as caveolae[24]. This is because the cholesterol-enriched flask-like membrane invaginations of caveolae may provide proper platforms for harboring and gating SAC[25-27], when caveolae rapidly flatten and disassemble in response to an increase in membrane tension[28,29]. As for Piezo1, structural analysis has shown that there is a pocket sandwiched between Piezo1 repeat B and C, which provides a binding site as a means of interaction with the lipids[14]. Despite such evidence of structure for lipid interaction, the localization of Piezo1 is not well established and thus it remains unclear whether its activity is regulated by caveolae.

In this study, we hypothesized that Piezo1 channels mediate the compression-enhanced invasive phenotype of cancer cells. To test this hypothesis, we examined *in vitro* cultured human breast cancer cells for their ability to invade and degrade extracellular matrix in the presence or absence of compressive stress, together with corresponding changes in Piezo1 and calcium signaling. We found that compressive stress promoted an invasive phenotype in the breast cancer cells, characterized by enhanced matrix degradation, actin protrusion formation, and calcium signal initiation. More importantly, the phenotypic changes in these cells appeared to be mediated by compression-induced Piezo1 activation, which in turn was dependent on the integrity of caveolae.

Results

Compressive stress enhanced invasion of breast cancer cells dependent on Piezo1

To test whether compressive stress enhances invasion of breast cancer cells, MDA-MB-231 cells were grown on 2D membrane filter (8 μm pore) coated with Matrigel and covered with a thin 1% agarose gel pad, and then exposed to a constant weight (Figure 1a). The compressive stress levels used in this study were 200, 400, and 600 Pa, which were considered pathophysiologically relevant as cells are reported to experience compressive stress at up to about 800 Pa in the core of the solid breast tumor[9,30]. As shown in Figure 1b and 1c, there were more MDA-MB-231 cells that invaded through the Matrigel-coated transwell filters when exposed to compressive stress compared to their un-compressed counterparts (control). The results clearly show that compressive stress enhanced breast cancer cell invasion in a pressure-dependent manner.

In order to test whether the compression-enhanced cancer cell invasion was mediated through SAC or more specifically through Piezo1, we first pretreated MDA-MB-231 cells with SAC inhibitors Gd^{3+} or more specific inhibitor GsMTx4, separately, followed by exposure to 400 Pa compressive stress. As shown in Figure 1d and 1e, pretreatment with Gd^{3+} or GsMTx4 either partially attenuated or completely abrogated compression-enhanced cancer cell invasion.

To further confirm the specificity of Piezo1 in mediating compression-enhanced cancer cell invasion, we first examined the expression of Piezo1 in MDA-MB-231 cells. We found that Piezo1 was expressed in MDA-MB-231 cells in the form of puncta structures and located not only on the plasma membrane, but also over the intracellular space and nucleus (Figure S1a), consistent with data reported by Gudipaty *et al*.[31]. We then silenced the protein expression of Piezo1 in MDA-MB-231 cells by using siRNA. Western blot results confirmed that the efficiency of Piezo1 knockdown (KD) was ~70% (Figure S1b). When MDA-MB-231 cells pretreated with Piezo1 siRNA were exposed to 400 Pa compressive stress, the enhanced cell invasion in response to compression was completely abrogated (Figure 1f and 1g). This supports Piezo1's function in compression-enhanced cancer cell invasion.

Compressive stress enhanced matrix degradation dependent on Piezo1

From the results thus far, we suspect compressive stress may influence cancer cells' capability for matrix degradation. To investigate this, we examined the extent of matrix degradation of MDA-MB-231 cells seeded on FITC-conjugated gelatin-coated glass bottom dish followed by application of compressive stress (Figure 2a). The fluorescence images showed dark puncta areas, corresponding to "holes" formed in the gelatin matrix due to degradation (Figure 2b). Thus, we quantified the extent of matrix degradation, and the results showed that MDA-MB-231 cells exposed to compressive stress from 200 Pa to 600 Pa exhibited a significant and pressure-dependent increase of gelatin matrix degradation as compared to their un-compressed counterparts (0 Pa) (Figure 2c). We sometimes found that the holes in the gelatin matrix do not coincide with the cell areas. We suspect this is due to the movement of the cells during the course of compression, since our fluorescent gelatin coating is very uniform in control conditions without cells. Similar as in the case of cell invasion through Matrigel-coated transwell filters, pretreatment of MDA-MB-231 cells with GsMTx4 to inhibit Piezo1 or siRNA probe to silence Piezo1 expression completely abrogated the compression-enhanced gelatin matrix degradation in breast cancer cells (Figure 2c). These data indicate that compressive stress enhanced the matrix degradation capability of breast cancer cells in a Piezo1 dependent manner.

Cancer cells are known to use invadopodia formed on the membrane to promote ECM degradation[32,22,33,34]. Thus, we examined whether compressive stress could promote invadopodia formation in MDA-MB-231 cells. We used immunofluorescence-labeled cortactin, a marker for invadopodia[35], to visualize and identify invadopodia as cortactin-positive actin puncta on the cell membrane (Figure S2a). The number of invadopodia per cell was manually counted and reported for MDA-MB-231 cells with or without pretreatment with siRNA probe to silence Piezo1, respectively, and with or without exposed compressive stress. The results show that compressive stress increased the number of invadopodia per cell in MDA-MB-231 cells, which was significantly abrogated by silencing Piezo1 (Figure S2b). Although more detailed characterization may be needed to definitively confirm the identity of these protrusions as invadopodia, these results demonstrate that breast cancer cells responded to

compressive stress with increased number of actin protrusions that may be responsible for ECM degradation.

Piezo1 mediated compression-induced remodeling of F-actin

Cells under compressive stress may reprogram their intracellular mechanical structures such as F-actin to acquire appropriate mechanical properties. To observe the response of F-actin to compressive stress, we generated a stable cell line expressing RFP-Lifeact and monitored the dynamics of F-actin in MDA-MB-231 cells upon exposure to compressive stress. We observed that compressive stress significantly promoted the formation of stress fibers at the cell cortex region in as early as 10 min in single and collective wild type cells (Figure 3a, top panel). In contrast, the compression-enhanced formation of stress fiber was largely inhibited in the Piezo1 KD cells (Figure 3a, bottom panel). Interestingly, by using 3D spinning disk confocal imaging we discovered actin protrusions at the apical side of the MDA-MB-231 cells when exposed to 600 Pa compressive stress (Figure 3b, top panel). The actin protrusions were reduced in the Piezo1 KD cells exposed to the same amount of compressive stress (Figure 3b, bottom panel).

To quantify the size of these actin protrusions, we first analyzed the size of microspheres of 0.1, 0.2, and 0.5 μm diameter, respectively (Figure S3a) and found that measured pixel values in the vertical direction were in a linear relationship with the sizes of these microspheres (Figure S3b). Using this relationship to calibrate the actin protrusion length, we found that the average length of the apical actin protrusions were about 0.7 μm, respectively (Figure S3c).

Such apical actin protrusions appeared to be similar to the above-mentioned invadopodia. To verify whether or not these apical actin protrusions might be invadopodia or not, we examined the agarose gel that covered cells during compression using immunofluorescence microscopy. We found that the apical actin protrusions that were stuck in the agarose gel colocalized with cortactin and Tks5 (Figure S3d). Then, we coated the agarose gel with FITC-conjugated gelatin and used it to cover the cells during compression. We found many dark puncta appeared in the

gelatin at the apical side of the cells (Figure S3e). These data together strongly suggest that the apical actin protrusions induced by compressive stress were similar, in both structure and function, to the invadopodia commonly found at the ventral side of the cells.

Piezo1 mediated compressive stress-induced calcium signaling

Recently, internal cell-generated forces have been shown to evoke localized Piezo1-dependent calcium flickers[17]. To determine whether an externally imposed force can elicit calcium signaling in a Piezo1-dependent manner, we labeled the cells with canonical calcium dye Fluo-4/AM or transiently transfected a calcium biosensor G-GECO and performed live cell imaging during application of compressive stress to MDA-MB-231 cells. As shown in Figure 4a, calcium signaling, as indicated by the fluorescence intensity of Fluo-4, was activated instantaneously upon exposure to compressive stress (**Video 1**). The peak magnitude of activation (the relative fluorescence intensity of Fluo-4) increased between ~1.3 to ~2.3 fold as the compressive stress increased from 200 Pa to 600 Pa (Figure 4b). These results were confirmed by using G-GECO (**Video 2**, Figure 4c and d). The peak magnitude of activation also increased from ~1.5 to ~3.5 fold as the compressive stress increased from 200 Pa to 600 Pa. The kinetics of calcium transients were different between the two indicators, likely due to the different affinity for calcium.

The G-GECO system was used to measure calcium signaling in the following experiments, as it is more convenient than the Fluo-4/AM system. To determine if calcium signaling was due to extracellular or intracellular calcium, we treated cells transfected with G-GECO with 2 mM EGTA for 15 min to deplete extracellular calcium content before application of compressive stress (400 Pa). Under this condition, we found that compressive stress-induced calcium signaling was abolished, suggesting the signaling was due to influx of extracellular calcium (Figure 4e). Furthermore, calcium influx induced by compressive stress (400 Pa) was also abrogated when cells were pretreated with Gd^{3+} or GsMTx4 to block Piezo1, or siRNA probe to silence Piezo1 expression (Figure 4f). Together, these observations support the finding that

Piezo1 mediated the cellular response to compressive stress *via* calcium influx.

Piezo1 mediated compression-enhanced Src/ERK activation

During invadopodia formation and maturation to degrade matrix, several signaling pathways are involved including Src/ERK pathways which promote the formation of invadopodia[23]. To test whether these signaling pathways are activated by compressive stress, we quantified the phosphorylation of ERK and Src in MDA-MB-231 cells following compression. We found that compressive stress significantly activated ERK and Src (Figure 5a). Additionally, Piezo1 KD effectively abolished the compressive stress-promoted signaling of Src, but not for ERK (Figure 5b), suggesting that Src, but not ERK was activated by compressive stress in a Piezo1 dependent manner.

Caveolae regulated the location and function of Piezo1

Previous work suggests that cholesterol content that directly influences the formation of caveolae might regulate Piezo1 functions[36-39]. Since caveolae assembly and disassembly have been tied to changes in membrane tension[29], we speculated that compressive stress activation of Piezo1 might also be dependent on caveolae. We first examined the spatial relationship between Piezo1 and caveolae. We found that both Piezo1 and caveolae formed puncta structures and many of them were colocalized (Figure 6a). The coefficient of colocalization in wild type cells was analyzed with Coloc2 procedure in Fiji software as shown in Figure 6b. The results show that classical Pearson coefficient was 0.76 ± 0.13, which indicates that Piezo1 and Cav-1 were highly colocalized. To test whether caveolae regulate the Piezo1 expression, we quantified Piezo1 protein expression level in wild type, Cav-1 EGFP transiently transfected, and Piezo1 KD MDA-MB-231 cells. We found that Cav-1 EGFP expression increased Piezo1 expression while Cav-1 KD decreased Piezo1 expression (Figure 6c).

To verify the role of caveolae in Piezo localization in the cell membrane, MDA-MB-231 was treated with 5 mM of MβCD that dramatically reduced the number of caveolae (Figure S4a). Consequently, the fluorescence intensity of Piezo1 decreased

in the cell membrane, but increased in the nucleus at the 5 min time point (Figure 6d), suggesting caveolae regulated Piezo1 localization in MDA-MB-231 cells.

To test the role of caveolae in regulating the function of Piezo1, cells were pretreated with either 5 mM MβCD or siRNA probe which silenced Cav-1 expression by about 60% (Figure S4b) and then exposed to compressive stress. We found that the compressive stress-induced calcium influx was blocked in both conditions (Figure S4c). Consistent with this results, Cav-1 KD also abrogated the compressive stress-enhanced cancer cell invasion (Figure S4d and S4e). Altogether, these data further support the idea that Piezo1 function may be dependent on caveolae.

Discussion

In the present study, we showed that in breast cancer cells, compressive stress enhanced cancer cell invasion, matrix degradation, and the formation of stress fiber and actin protrusion. Additionally, we identified that Piezo1 mediated these processes and the invasive phenotypes also depended on the integrity of caveolae. These findings provide the first demonstration that compressive stress enhances matrix degradation by breast cancer cells and that Piezo1 is an essential mechanosensor and transducer for such stress in breast cancer cells.

Invasion of cells through ECM is a critical activity during cancer metastasis. Uncontrolled growth-induced compressive stress triggers invasive phenotype by forming leader cells[9]. It is, however, unknown whether such stress would affect the capability of cancer cells to induce ECM degradation. It is also known that the ability of forming actin protrusions such as invadopodia is directly correlated with their invasive potential in breast cancer cells[32]. Consistent with enhanced invasion under compressive stress, we found compressive stress enhanced matrix degradation *via* promoting actin protrusions in both apical and ventral side of breast cancer cells. Thus, it is plausible that compressive stress in solid tumor might initiate the invasion by enhancing the capability of matrix degradation *via* actin protrusions. If that is the case *in vivo*, compressive stress might promote cancer cells to ‘dig more holes’ in the basement membrane which provide a way for their metastasis.

While it is known that compressive stress affects cancer progression, how cancer cells sense and respond to such stress is not completely understood. Under compressive stress, cell membrane will be stretched which, in turn, increases the membrane tension. Piezo channels are the most notable family of SAC in mammalian cells which are gated by membrane tension[40]. It has been found that Piezo1 channels play essential roles in diverse physiological and pathological processes including cell migration[41,42] and the Piezo1 mRNA expression level is highly correlated with the reduced overall survival of breast cancer patients[20]. Our study also confirmed that Piezo1 channels are essential in mediating the invasion of breast cancer cells.

Emerging evidence indicate that caveolae harbor and modulate ion channels. TRPV1 channels expression and distribution on the plasma membrane can be disrupted by the removal of caveolae *via* cholesterol depletion[43]. Similar to TRPV1, we found Piezo1 behaves similarly by shifting its localization to the nucleus upon cholesterol depletion. Interestingly, in stretch-triggered mitosis, Piezo1 was also observed to localize to the nuclear envelope[31]. Thus, it may be a general strategy where a functional relationship between caveolae and Piezo1 regulates force sensing and our data supports the model where caveolae might be the “mechanical force foci” which concentrates Piezo1 to facilitate force sensing and transduction in mammalian cells.

The mechanisms of how Piezo1 channels are gated by mechanical stress is still unclear. Piezo1 channels appear to sense tension in the bilayer and are gated according to “force-from-lipid” principle, an evolutionally conserved gating mechanism[44]. According to this paradigm, the activity and sensitivity of Piezo1 channels can be regulated by lipid membrane. The physical properties of lipid membrane such as thickness, stiffness, and lateral pressure profile found within caveolae may be different from the surrounding membrane. For instance, disruption of caveolae by cholesterol depletion has been demonstrated to change membrane stiffness[36] and results in suppression of epithelial sodium channels and TRP channels[38,45]. In this context, it is plausible that cholesterol-enriched caveolae might affect sensitivity of Piezo1 *via* controlling the membrane pressure profile. Stomatin-like

protein-3 has been reported to tune the sensitivity of Piezo1 channels by controlling the membrane mechanical properties through recruiting cholesterol[36,46]. In this study, we found that the function of Piezo1 in compressive stress sensing is regulated by caveolae. Taken together, it is likely that Piezo1 is located in cholesterol-rich caveolae microdomains and caveolae integrity regulates Piezo1 function.

In addition to membrane structures, cells experiencing mechanical stress can also reorganize their cytoskeletal structures to adapt to a new mechanical microenvironment. Among them, stress fibers are essential cellular structures that control various cellular behaviors. Reports have shown that mechanical tension induces the assembly of stress fibers[47]. In this study, we found that cells under compressive stress quickly assembled new stress fibers in as early as 10 min. This may be to increase their cellular mechanical strength to balance compressive stress.

Our results also demonstrate the regulatory roles of several key pathways of mechanotransduction in the compression-enhanced cancer cell invasive phenotype including Src, ERK and calcium, which are pathways linked to the formation and function of actin protrusion such as invadopodia[48,49]. Our study thus provides a comprehensive understanding from disparate systems in the context of compression-enhanced breast cancer cell invasion (Figure 7).

It is worthy to note that, in this study, we only evaluated the effect of uniaxial compressive stress on breast cancer cells in a 2D culture model. However, cells *in vivo* grow and live in a 3D microenvironment, which may impact the force direction and change the dynamic response of the cells to compression. Additionally, we only assayed cell invasion in response to compressive stress. Many other features of breast cancer cells such as the loss of acini morphologies in response to compression still need to be explored. For instance, Ricca *et al.* have shown that brief compression to single malignant breast cancer cell in laminin-rich ECM can stimulate the formation of acinar-like structures, indicating that compressive stress may cause malignancy reversion in breast cancer cells[50]. Furthermore, we just investigated the role of Piezo1 in mediating the breast cancer cell response to compressive stress. However, as another family member, Piezo2 has also been reported to express in these cells[51],

raising the question of its potential implication. Therefore, further studies are required in order to fully elucidate the behaviors and associated underlying mechanisms of breast cancer cells in response to compressive stress during tumor growth and metastasis.

In conclusion, our work may have relevance to human tumors *in vivo*. As solid tumor experiences high compressive stress due to uncontrolled proliferation and confinement by the stiff extracellular matrix environment, this microenvironment facilitates compression-enhanced cell invasion. The identification of Piezo1's crucial role in this process provides the first demonstration of the dependence of Piezo1 channels on the response of breast cancer cells to physiological compressive stress. Both of these findings underscore the cardinal role that Piezo1 channels play in regulating cell invasion and may inspire further development targeting Piezo1 as a potential cancer therapeutic target.

Materials and Methods

Cell culture and preparation

MDA-MB-231 cells (ATCC HTB-26), an invasive breast adenocarcinoma cell line, were cultured in DMEM with 2 mM L-glutamine (# 11965-092, Thermo Fisher, MA) supplemented with 10% fetal bovine serum (FBS, # 35-010-CV, Thermo Fisher, MA), 100 units/ml penicillin, 100 µg/ml streptomycin, 2.5 µg/ml Fungizone, and 5 µg/ml gentamicin (# 15750-060, Invitrogen, MA) at 5% CO_2 and 37 °C. MCF10A (ATCC® CRL-10317™) cells, a normal breast cell line, were cultured in DMEM/Ham's F-12 (Gibco-Invitrogen, Carlsbad, CA) supplemented with 100 ng/ml cholera toxin, 20 ng/ml epidermal growth factor (EGF; # PHG0311, Invitrogen, MA), 0.01 mg/ml insulin, 500 ng/ml hydrocortisone, and 10% FBS. For matrix degradation and invadopodia experiments, cells were incubated in invadopodia medium containing DMEM supplement with 5% Nu-Serum (# 355104, Corning, NY), 10% FBS, and 20 ng/ml EGF.

For labeling actin in live cells, stable cell lines expressing Lifeact-RFP were generated *via* lentiviral transfection. The lentiviral transfer plasmids pLVX-puro-GFP-Lifeact and pLVX-puro-RFP-Lifeact were cloned from RFP-Lifeact plasmid obtained

from Dr. Gaudenz Danuser (UT-Southwestern). Briefly, lentiviruses were produced by transfecting human embryonic kidney (HEK)-293T cells with psPAX2 and pMD2.G (Addgene) and pLVX-puro-GFP-Lifeact viral vectors. Conditioned medium containing viruses was collected after 5 days and then used immediately to infect cells or stored at −80 °C. Transduced target cells were selected with puromycin for 72 h.

For optical imaging of dynamic calcium signaling and caveolae localization in live cells, cell lines transiently expressing G-GECO (a green fluorescent genetically encoded calcium indicator) and caveolin-1 (Cav-1)-EGFP respectively were generated *via* plasmid transfection. The plasmids expressing G-GECO was a generous gift from Takanari Inoue (Johns Hopkins University)[52], and those expressing Cav-1-EGFP were from Ari Helenius (ETH Zurich). Briefly, cells were transfected with Lipofectamine-2000 (# 11668-019, Life Technologies). For 35 mm glass bottom dishes, 6 μg plasmid DNA in Optimem® transfection medium (# 31985062, Gibco) was used for each transfection. After 24 h at 37 °C, the transfection medium was replaced with complete medium, and cells were processed after 24-48 h later.

In vitro compression device

To investigate the effect of compressive stress on cell behaviors, we used a previously described setup[9,53]. Briefly, cells were grown either in a 35 mm culture dish with glass bottom (# 12-565-90, Fisher Scientific) that was coated with/without gelatin, or in a transwell chamber with permeable membrane of 8-μm pores that was coated with Matrigel. Then the cells were covered with a soft agarose disk layer, and subsequently a piston of specific weight was placed on top of the agarose disk to apply a given compressive stress to the cells underneath indirectly. The cross-sectional area of the piston (24 mm diameter) was 4.52 cm^2 but its weight was variable at 9.22 g, 18.45 g, and 27.67 g, corresponding to a stress of 200 Pa, 400 Pa, and 600 Pa, respectively, on the cells. Cells prepared as such but not subjected to piston weight were used as controls.

In vitro transwell invasion assay

To assay the effect of compressive stress on cell invasion, standard transwell invasion assay adapted from Bravo-Cordero[54,55] was performed using 6-well Transwell chambers that were separated as upper and lower chambers by filter membrane with 8 μm pores (# 07-200-169, Corning). For the assay, the transwell filter membrane was coated with 300 μl Matrigel (12 mg/ml, # E1270, Sigma, Burlington, MA) diluted in serum-free DMEM (2 mg/ml final concentration), followed by incubation for 1 h at 37 °C. MDA-MB-231 cells in serum-free medium (5×10^5 cells/well) were placed in the upper chamber, while the lower chamber was filled with 2 ml complete medium. Cells were allowed to grow for 6 h and then compressed for 18 h before being fixed with 4% paraformaldehyde (# 30525-89-4, Electron Microscopy Sciences, Hatfield, PA). The non-invasive cells on the upper chamber were removed with cotton swabs, and the invaded cells in the lower chamber were stained with 0.1% crystal violet (# C6158; Sigma) for 10 min at room temperature, prior to being examined and imaged by light microscopy at 10× magnification (Olympus BX60; Olympus Corporation, Tokyo, Japan). Then the number of stained cells in the lower chamber was counted using ImageJ software (National Institute of Health, Bethesda, MD) and the enhancement of cellular invasion induced by compressive stress was quantified as percentage (%) of the number of compressed cells over that of the non-compressed cells that had invaded through the filter membrane, *i.e.* [# of cells in the lower chamber in the presence of a specific weight (experiment group)]/[# of cells in the lower chamber in the absence of a specific weight (control group)]. Results are based on the analysis of 10 random fields per transwell in each condition and each experiment was repeated three times.

Evaluation of invadopodia formation and ECM degradation

To determine whether compressive stress enhances cells' ability to degrade ECM, we examined cells cultured on gelatin substrate for their tendency to form invadopodia and associated gelatin degradation, according to a protocol adapted from Artym *et al.* [56]. Briefly, glass bottom dishes were treated with 20% nitric acid for 1 h, washed with H_2O for 4 times, then incubated with 50 μg/ml poly-L-lysine (# P8920, Sigma) in PBS for 15 min and washed with PBS, then further incubated with 0.5% glutaraldehyde in

PBS on ice for 15 min followed by thorough washes with PBS. Subsequently, the dishes were coated with 1 ml of gelatin in PBS (1: 9 of 0.1% fluorescein isothiocyanate (FITC)-gelatin (# G13186, Invitrogen, MA): 2% porcine gelatin), then washed in PBS, incubated with 5 mg/ml sodium borohydride ($NaBH_4$) for 3 min, rinsed in PBS, and then incubated in 10% calf serum/DMEM at 37° for 2 h. Afterwards, cells were seeded in each dish at $5x10^5$ cells per well and incubated for 8 h, and then subjected to compressive stress of either 200 Pa, 400 Pa, or 600 Pa, respectively, for 8 h as aforementioned.

Upon completion of compression, the cells were imaged with live fluorescence microscopy (at 60x) and the microscopic images were analyzed by using ImageJ to assess the formation of invadopodia and the degradation of gelatin matrix. Invadopodia were defined as F-actin-positive puncta protruding from the cells into the gelatin matrix underneath the cell in our experiments[57]. For each independent experiment that was performed in triplicates, the number of invadopodia per cell was quantified with cells imaged randomly in >15 microscope view fields, representing a total of ~100 cells per experimental condition. At the same time, the degradation of gelatin matrix was quantified as the percentage of degraded area (dark spots comprised of dense degraded protein products) in the whole area underneath each cell.

Live fluorescence microscopy

To observe the dynamics of actin, Cav-1, and calcium signaling, live cells expressing Lifeact-RFP, Cav-1-EGFP, and G-GECO were imaged with a spinning disk confocal microscope with a 60x or 100x oil immersion objective (Olympus IX73 with Yokogawa CSU-X1). For live fluorescence microscopy, cells were seeded in a 35 mm glass bottom dish that was placed in an environmental chamber mounted on the microscope to maintain constant 37 °C, 5% CO_2, and humidity. Cav-1-EGFP was observed at the excitation wavelength of 488 nm. For dynamic tracking of actin in live cells, the cells were consecutively imaged for up to 60 min, and the images were processed using ImageJ. Cells were observed from both top-down and side view for

spatial localization of actin, and caveolae by 3D reconstruction of images in Z-stacks (0.4 μm increments for 60x objective and 0.2 μm increments for 100x objective).

To quantify the size of the apical actin protrusion, microspheres of different diameters (0.1, 0.2 and 0.5 μm; cat # F8801, F8810, F8812, ThermoFisher, respectively) were laid flat on the glass cover slip and imaged with the abovementioned methods for imaging actin. We then analyzed the relationship between the measured pixel size in the vertical direction of these microspheres and the actual diameters of these microspheres. We made sure that a linear relationship was established. Then, we used this linear relationship to analyze the length of the upward actin protrusions based on the pixel size of the imaged actin protrusions.

Intracellular Ca^{2+} measurement

To evaluate the intracellular calcium concentration ($[Ca^{2+}]$), we used cells labeled with Fluo-4/AM (# F14201, Thermo Fisher) or transiently expressed with calcium-sensitive reporter G-GECO[58] and then evaluated the intensity of intracellular calcium signaling. For the Fluo-4/AM system, cells were incubated with Fluo-4/AM for 1 h at room temperature (25 ± 2 °C) followed by a 0.5 h wash at 37 °C. For the G-GECO system, cells transfected with G-GECO for 48 h were plated into a glass bottom dish, which was further incubated for 24 h. Subsequently, the cells were imaged on a spinning disk confocal microscope (60 x objective), with fluorescence excitation and emission at 488 nm and 533 nm, respectively. For each experimental group, twenty cells were randomly selected and the fluorescence intensity per cell was quantified using ImageJ.

Drug treatments

For experiments involving inhibitors, cells were exposed to inhibitor for 0.5 h, unless stated otherwise, in presence or absence of compressive stress. For inhibiting the function of mechanically sensitive ion channels, cells were treated with Gadolinium chloride (Gd^{3+}, 5 μM, # 203289, Sigma, Burlington, MA) or GsMTx4 (5 μM, #ab141871; Abcam, Cambridge, MA). To remove calcium ion from the DMEM, EGTA (2 mM, #

E3889; Sigma, Burlington, MA) was added to the medium. To disrupt caveolae in the membrane, cells were treated with 5 mM of methyl-β-cyclodextrin (MβCD, # SLBP3372V, Sigma, Burlington, MA).

Antibodies for immunoblotting and Western blot

Antibodies used in immunofluorescence and Western blot include: anti-Tks5 polyclonal antibody (# 09-403-MI), anti-GAPDH mouse monoclonal antibody (# CB1001) purchased from EMD Millipore (Billerica, MA); anti-Src rabbit antibody (# 2108), anti-p-Src (Y416) rabbit antibody (# 2101), anti-p44/42 MAPK (ERK1/2) mouse monoclonal antibody (# 4696), and anti-p-ERK1/2 (Thr202Tyr204) rabbit monoclonal antibi (# 4370) obtained from Cell Signaling Technology (Danvers, MA), respectively; anti-cortactin rabbit monoclonal antibody (# Ab81208) purchased from Abcam (Cambridge, MA); Cav-1 rabbit polyclonal antibody (# PA1-064) obtained from Thermo Fisher (Grand Island, NY).

RNA interference

To silence the expression of Piezo1 and Cav-1, Negative Control Medium GC Duplex #2 and siRNA interference for Piezo1 (# AM16708, Assay ID:138387, Thermo Fisher) and Cav-1 (# AM16708, Assay ID: 10297, Thermo Fisher) were used. Briefly, Cells were seeded in 6-well plates at 1×10^6 cells/well for 24 h prior to transfection. At 90% confluence the cells were transfected with 30 nmol/L siRNA using Lipofectamine RNAi MAX (# 13778, Invitrogen, MA) in OptiMEM according to the manufacturer's instructions. Transfection mixes were applied to the cells for 24 h, subsequently removed and replaced with 2 ml of growth media. The cells were cultured for 48 h before use in experiments. The protein expression levels of Piezo1 and Cav-1 were ascertained by Western blotting.

Immunofluorescence and colocalization analysis

Cells were fixed with 4% paraformaldehyde for 10 min and permeabilized with 0.1 % TritonX-100 for 10 min at room temperature. Non-specific sites were blocked using 5 %

non-fat milk in PBS for 1 h at room temperature. Cells were then incubated in 5 % non-fat milk in PBS containing primary antibodies at 1:100 dilution for 1 h at room temperature. After washing with PBS, cells were incubated with Alexa Fluor 594 or 640 conjugated secondary antibody for 60 min at room temperature. Cells were visualized using the spinning disk confocal microscope with 60x oil immersion objective. For F-actin staining, cells were incubated with 1:100 rhodamine phalloidin (# PHDR1, Cytoskeleton Inc.) for 60 min at room temperature.

Colocalization of Piezo1 and Cav-1 was analyzed using Fiji software [59] containing a procedure for colocalization analysis, designated as Coloc2, which are based on pixel-intensity-correlation measurements. Pearson coefficient and 2D intensity histograms were recorded to quantify the degree of the colocalization between Piezo1 and Cav-1.

Western blotting

Western blot assay was used to examine the protein expression and/or activity of Piezo1, Cav-1, Src, and ERK. Cells grown on glass bottom dishes under described assay conditions were lysed using RIPA buffer (# R0278, Sigma) with added cocktail of protease and phosphatase inhibitors (MS-SAFE, Sigma). Protein concentration of cell lysates were determined using the Protein Assay Reagent (#23227, Thermo Fisher Scientific, Waltham, MA). Cell lysis buffer was combined in 4× SDS sample buffer and 2-mercaptoethanol and incubated at 95 °C for 5 min. After loading equal amount of protein per lane, SDS-PAGE was performed. The proteins were transferred onto 0.22 μm nitrocellulose membranes (# 66485, Pall Life Sciences) using Pierce G2 Fast Blotter (Thermo Fisher Scientific, Waltham, MA). Following transfer, the membranes were blocked using 5% nonfat milk in 1x TBST (Tris-buffered saline and 0.1% of Tween-20) for 1 h at RT with gentle agitation and incubated with the primary antibodies overnight at 4 °C under mild shaking condition. After washing three time with 1x TBST, membranes were incubated with goat anti-rabbit secondary antibody (DyLight 800, # SA5-10036, Thermo Fisher) or goat anti-mouse secondary antibody (DyLight 680, # 35518, Thermo Fisher) at RT for 1 h. Signal of immunoblots were detected using the

Odyssey Infrared Imaging system (LI-COR, Lincoln, NE). For quantification, intensity of gel band was calculated after subtracting the background. The relative protein expression was expressed as a ratio of the band intensity to that of the control group after both of them were normalized to that of GAPDH.

Statistical analysis

Statistical analysis was done using one-way analysis of variance (ANOVA), followed by post-hoc multiple comparisons. Statistical significance set to $*p < 0.05$ and $**p < 0.01$. All experiments were repeated at least three times and the data were expressed as means ± s.e.m. (standard error of the mean), unless otherwise noted.

Declarations

Ethics approval and consent to participate: Does not apply

Consent for publication: All authors have consented to publication

Availability of data and materials: All raw data and reagents generated from this work will be made available upon request.

Competing interests: The authors declare no competing interests in relation to the work described.

Funding: Funding for the work was provided by the Key Program of NSF of China (No. 11532003) to L.D.. M.L. is supported by Jiangsu Oversea Visiting Scholar Program for University Prominent Young and Middle-aged Teachers and Presidents. A.P.L. is supported by NSF-MCB 1561794.

Author contributions statement: M.L conceived, designed, and performed the experiments, analyzed the data, prepared figures, and wrote the manuscript. K.H., Z.T., and L.D. revised the manuscript. A.P.L. conceived the study and wrote the manuscript. All authors reviewed the manuscript.

Acknowledgements: We thank Takanari Inoue (Johns Hopkins University) for providing the G-GECO plasmid. The technical assistance from Shue Wang and Maxwell DeNies is gratefully acknowledged.

Figure captions

Figure 1 Compressive stress enhanced invasion of MDA-MB-231 cells depending on Piezo1. Cell invasion was measured with *in vitro* transwell invasion assay. **a** Schematic diagram of the compression experiment using a transwell setup. Cells grown on membrane filter (8 μm pore) coated with Matrigel for 6 h were covered with 1% of agarose gel and compressed with a specific weight. **b, c** Representative images of invaded cells stained with crystal violet under different compressive stress and quantification of percentage of invaded cells. **d**, **e** Representative images of invaded cells and quantification of percentage of invaded cells treated with Gadolinium chloride (Gd^{3+}) or GsMTx4 under 400 Pa. **f**, **g** Representative images of invaded cells and quantification of percentage of invaded cells treated with siRNA for Piezo1 under 400 Pa. Dashlines in **c** indicate cell invasion under 400 Pa without any perturbations, n = 3. $^{*}p < 0.05$ versus control groups; ** $p < 0.01$ versus control groups. Error bars represent s.e.m..

Figure 2 Compressive stress promoted matrix degradation in MDA-MB-231 cells. **a** Schematic diagram of the experiment. Cells grown on a glass-bottom dish coated with FITC-conjugated gelatin for 8 h were covered with 1% of agarose gel and compressed with a specific weight. **b** Representative images (red: actin, green: gelatin) of compression-promoted gelatin degradation at the ventral side of the cell. Gelatin degradation was visualized by confocal microscopy as disappearance of green fluorescence. The arrow in 200 Pa shows an example of the punctate gelatin-degraded region. Insets of 600 Pa images are magnified view of the boxed regions. **c** The fold change of gelatin degradation area under different treatment conditions as a function of compressive stress normalized to gelatin degradation area at 0 Pa. ** $p < 0.01$ versus control groups. Error bars represent s.e.m..

Figure 3 Piezo1 mediated compressive stress-induced formation of stress fiber and actin protrusions. **a** Representative images of stress fiber at the ventral side of MDA-

MB-231 cells expressing Lifeact-RFP with (600 Pa, bottom panel) or without Piezo KD under compression (600 Pa, upper panel with single cell or collective cells) for 60 min (white arrows in the images show the stress fiber formation). **b** Representative images of actin protrusions at the apical side of MDA-MB-231 cells expressing Lifeact-RFP under compression (600 Pa) for 60 min (see magnified views and yellow arrow heads in the images at 30 and 60 min).

Figure 4 Compressive stress induced calcium signaling in MDA-MB-231 cells. Representative images of intracellular [Ca^{2+}] (**a** and **c**) and average time-courses of changing relative mean fluorescence intensity (**b** and **d**) of Fluo-4 or G-GECO (normalized to time 0) in MDA-MB-231 cells labeled with Fluo-4/AM or transiently expressing G-GECO before (0 min) and after (1 min) exposure to compressive stress at 200, 400, 600 Pa, respectively. **e, f** Time-courses of changing relative mean fluorescence intensity of G-GECO in MDA-MB-231 cells pretreated with or without EGTA, Gd^{3+}, GsMTx4, and Piezo1 KD in response to 400 Pa compressive stress. Each experiment assayed 10-20 cells and repeated three times.

Figure 5 Compression enhanced the activity of ERK and Src. **a** The phosphorylation of ERK and Src in MDA-MB-231 cells pretreated with scramble probes in the absence or presence of compressive stress at 200, 400, 600 Pa. **b** The phosphorylation of ERK and Src in MDA-MB-231 cells pretreated with siRNA for Piezo1 in the absence or presence of compressive stress at 200, 400, 600 Pa. Relative phosphorylation levels were obtained by normalizing to GAPDH expression and 0 Pa value, n = 3. $^{*}p < 0.05$ versus control groups; $^{**}p < 0.01$ versus control groups. Error bars represent s.e.m..

Figure 6 The expression and distribution of Piezo1 in MDA-MB-231 cells were regulated by caveolae. **a** Representative fluorescence images of Piezo1 (magenta) and caveolae (green) colocalization and 2D intensity histogram output in MDA-MB-231 cells. Insets in both conditions show magnified view of the boxed regions. **b** Representative image of 2D intensity histogram output of Coloc2 analysis performed

using Fiji software. The text indicates the Pearson coefficient (± SD) of the pixel-intensity correlation (n = 8). **c** Western blot images and quantification of Piezo1 expression in wield type (WT), Cav-1 EGFP expressing, and Cav-1 KD MDA-MB-231 cells (n = 3). $^{*}p < 0.05$ versus control groups; $^{**}p < 0.01$ versus control groups. **d**, Representative fluorescence images of Piezo1 (green) and nucleus (blue) after cells were treated with MβCD for 5 min, 10 min, and 20 min (upper panel: *x*-*y* view, lower panel: *x*-*z* view). Error bars represent s.e.m..

Figure 7 Model of compressive stress-promoted invasive phenotype of MDA-MB-231 cells and associated signaling pathways. Together, vertical mechanical compressive stress increases the lateral plasma membrane tension and activates Piezo1 channels. The opening of Piezo1 mediates the influx of calcium and evokes downstream signaling pathways such as Src. These activated signaling molecules promote actin protrusions both at the apical and ventral sides of cells and the remodeling of actin cytoskeleton, which in turn mediate enhanced matrix degradation and cell invasion.

Reference

1 Liu, A. P., Chaudhuri, O. & Parekh, S. H. New advances in probing cell-extracellular matrix interactions. *Integrative biology: quantitative biosciences from nano to macro* **9**, 383-405, doi:10.1039/c6ib00251j (2017).

2 Stylianopoulos, T., Munn, L. L. & Jain, R. K. Reengineering the physical microenvironment of tumors to improve drug delivery and efficacy: from mathematical modeling to bench to bedside. *Trends in Cancer* **4**, 292-319, doi:10.1016/j.trecan.2018.02.005 (2018).

3 Petrie, R. J., Harlin, H. M., Korsak, L. I. T. & Yamada, K. M. Activating the nuclear piston mechanism of 3D migration in tumor cells. *The Journal of Cell Biology*, doi:10.1083/jcb.201605097 (2016).

4 Wirtz, D., Konstantopoulos, K. & Searson, P. C. The physics of cancer: the role of physical interactions and mechanical forces in metastasis. *Nature Reviews Cancer* **11**, 512, doi:10.1038/nrc3080 (2011).

5 . (!!! INVALID CITATION !!! 5).

6 Ariffin, A. B., Forde, P. F., Jahangeer, S., Soden, D. M. & Hinchion, J. Releasing pressure in tumors: what do we know so far and where do we go from here? A review. *Cancer Research* **74**, 2655-2662, doi:10.1158/0008-5472.can-13-3696 (2014).

7 Stylianopoulos, T. The solid mechanics of cancer and strategies for improved therapy. *Journal of Biomechanical Engineering* **139**, 021004, doi:10.1115/1.4034991 (2017).

8 Johanna Heureaux-Torres, K. E. L., Henry Haley, Matthew Pirone, Lap Man Lee, Yoani Herrera, Gary D. Luker, and Allen P. Liu. The effect of mechanosensitive channel MscL expression in cancer cells on 3D confined migration. *APL Bioengineering* **2**, 032001, doi:10.1063/1.5019770 (2018).

9 Tse, J. M. *et al.* Mechanical compression drives cancer cells toward invasive phenotype. *Proceedings of the National Academy of Sciences* **109**, 911-916, doi:10.1073/pnas.1118910109 (2012).

10 Tao, J. & Sun, Sean X. Active biochemical regulation of cell volume and a simple model of cell tension response. *Biophysical Journal* **109**, 1541-1550, doi:10.1016/j.bpj.2015.08.025 (2015).

11 Coste, B. *et al.* Piezo1 and Piezo2 are essential components of distinct mechanically activated cation Channels. *Science* **330**, 55-60, doi:10.1126/science.1193270 (2010).

12 He, L. *et al.* Role of membrane-tension gated Ca(2+) flux in cell mechanosensation. *Journal of cell science* **131**, doi:10.1242/jcs.208470 (2018).

13 Zhao, Q. *et al.* Structure and mechanogating mechanism of the Piezo1 channel. *Nature* **554**, 487, doi:10.1038/nature25743 (2018).

14 Saotome, K. *et al.* Structure of the mechanically activated ion channel Piezo1. *Nature* **554**, 481-486, doi:10.1038/nature25453 (2018).

15 Lewis, A. H. & Grandl, J. Mechanical sensitivity of Piezo1 ion channels can be tuned by cellular membrane tension. *eLife* **4**, e12088, doi:10.7554/eLife.12088 (2015).

16 Syeda, R. *et al.* Piezo1 channels are inherently mechanosensitive. *Cell reports* **17**, 1739-1746, doi:10.1016/j.celrep.2016.10.033 (2016).
17 Ellefsen, K. L. *et al.* Myosin-II mediated traction forces evoke localized Piezo1-dependent Ca(2+) flickers. *Commun Biol* **2**, 298, doi:10.1038/s42003-019-0514-3 (2019).
18 Nourse, J. L. & Pathak, M. M. How cells channel their stress: Interplay between Piezo1 and the cytoskeleton. *Semin Cell Dev Biol* **71**, 3-12, doi:10.1016/j.semcdb.2017.06.018 (2017).
19 Zeng, W.-Z. *et al.* PIEZOs mediate neuronal sensing of blood pressure and the baroreceptor reflex. *Science* **362**, 464-467, doi:10.1126/science.aau6324 (2018).
20 Li, C. *et al.* Piezo1 forms mechanosensitive ion channels in the human MCF-7 breast cancer cell line. *Scientific reports* **5**, 8364, doi:10.1038/srep08364 (2015).
21 Weng, Y. *et al.* PIEZO channel protein naturally expressed in human breast cancer cell MDA-MB-231 as probed by atomic force microscopy. *AIP Advances* **8**, 055101, doi:10.1063/1.5025036 (2018).
22 Mrkonjic, S., Destaing, O. & Albiges-Rizo, C. Mechanotransduction pulls the strings of matrix degradation at invadosome. *Matrix Biology* **57-58**, 190-203, doi:https://doi.org/10.1016/j.matbio.2016.06.007 (2017).
23 Burger, K. L. *et al.* Src-dependent Tks5 phosphorylation regulates invadopodia-associated invasion in prostate cancer cells. *The Prostate* **74**, 134-148, doi:10.1002/pros.22735 (2014).
24 Anishkin, A. & Kung, C. Stiffened lipid platforms at molecular force foci. *Proceedings of the National Academy of Sciences of the United States of America* **110**, 4886-4892, doi:10.1073/pnas.1302018110 (2013).
25 Teng, J., Loukin, S., Anishkin, A. & Kung, C. The force-from-lipid (FFL) principle of mechanosensitivity, at large and in elements. *Pflügers Archiv - European Journal of Physiology* **467**, 27-37, doi:10.1007/s00424-014-1530-2 (2015).
26 Park, S. W. *et al.* Caveolar remodeling is a critical mechanotransduction mechanism of the stretch-induced L-type Ca2+ channel activation in vascular myocytes. *Pflügers Archiv - European Journal of Physiology* **469**, 829-842, doi:10.1007/s00424-017-1957-3 (2017).
27 Lockwich, T. P. *et al.* Assembly of Trp1 in a sgnaling complex associated with caveolin-scaffolding lipid raft domains. *Journal of Biological Chemistry* **275**, 11934-11942, doi:10.1074/jbc.275.16.11934 (2000).
28 Yang, L. & Scarlata, S. Super-resolution visualization of caveola deformation in response to osmotic stress. *The Journal of Biological Chemistry* **292**, 3779-3788, doi:10.1074/jbc.M116.768499 (2017).
29 Sinha, B. *et al.* Cells respond to mechanical stress by rapid disassembly of caveolae. *Cell* **144**, 402-413, doi:10.1016/j.cell.2010.12.031 (2011).
30 Butcher, D. T., Alliston, T. & Weaver, V. M. A tense situation: forcing tumour progression. *Nature reviews. Cancer* **9**, 108-122, doi:10.1038/nrc2544 (2009).
31 Gudipaty, S. A. *et al.* Mechanical stretch triggers rapid epithelial cell division

through Piezo1. *Nature* **543**, 118-121, doi:10.1038/nature21407 (2017).
32 Paterson, E. K. & Courtneidge, S. A. Invadosomes are coming: new insights into function and disease relevance. *The FEBS journal*, doi:10.1111/febs.14123 (2017).
33 Parekh, A. & Weaver, A. M. Regulation of invadopodia by mechanical signaling. *Experimental cell research* **343**, 89-95, doi:10.1016/j.yexcr.2015.10.038 (2016).
34 Parekh, A. *et al.* Sensing and modulation of invadopodia across a wide range of rigidities. *Biophysical Journal* **100**, 573-582, doi:10.1016/j.bpj.2010.12.3733 (2011).
35 Sala, K., Raimondi, A., Tonoli, D., Tacchetti, C. & de Curtis, I. Identification of a membrane-less compartment regulating invadosome function and motility. *Scientific reports* **8**, 1164, doi:10.1038/s41598-018-19447-2 (2018).
36 Qi, Y. *et al.* Membrane stiffening by STOML3 facilitates mechanosensation in sensory neurons. *Nature communications* **6**, 8512-8512, doi:10.1038/ncomms9512 (2015).
37 Ridone, P. *et al.* Human Piezo1 membrane localization and gating kinetics are modulated by cholesetrol levels. *Biophysical Journal* **112**, 533a, doi:https://doi.org/10.1016/j.bpj.2016.11.2883 (2017).
38 Levitan, I., Fang, Y., Rosenhouse-Dantsker, A. & Romanenko, V. Cholesterol and ion channels. *Sub-cellular biochemistry* **51**, 509-549, doi:10.1007/978-90-481-8622-8_19 (2010).
39 Balijepalli, R. C. & Kamp, T. J. Caveolae, ion channels and cardiac arrhythmias. *Progress in biophysics and molecular biology* **98**, 149-160, doi:10.1016/j.pbiomolbio.2009.01.012 (2008).
40 Parpaite, T. & Coste, B. Piezo channels. *Current Biology* **27**, R250-R252, doi:https://doi.org/10.1016/j.cub.2017.01.048 (2017).
41 Maneshi, M. M., Ziegler, L., Sachs, F., Hua, S. Z. & Gottlieb, P. A. Enantiomeric Abeta peptides inhibit the fluid shear stress response of PIEZO1. *Scientific reports* **8**, 14267, doi:10.1038/s41598-018-32572-2 (2018).
42 Hung, W.-C. *et al.* Confinement Sensing and Signal Optimization via Piezo1/PKA and Myosin II Pathways. *Cell reports* **15**, 1430-1441, doi:https://doi.org/10.1016/j.celrep.2016.04.035 (2016).
43 Liu, M., Huang, W., Wu, D. & Priestley, J. V. TRPV1, but not P2X, requires cholesterol for its function and membrane expression in rat nociceptors. *The European journal of neuroscience* **24**, 1-6, doi:10.1111/j.1460-9568.2006.04889.x (2006).
44 Cox, C. D. *et al.* Removal of the mechanoprotective influence of the cytoskeleton reveals PIEZO1 is gated by bilayer tension. *Nature communications* **7**, 10366-10366, doi:10.1038/ncomms10366 (2016).
45 Huang, H., Bae, C., Sachs, F. & Suchyna, T. M. Caveolae regulation of mechanosensitive channel function in myotubes. *PloS one* **8**, e72894, doi:10.1371/journal.pone.0072894 (2013).
46 Poole, K., Herget, R., Lapatsina, L., Ngo, H. D. & Lewin, G. R. Tuning Piezo ion channels to detect molecular-scale movements relevant for fine touch. *Nat*

Commun **5**, 3520, doi:10.1038/ncomms4520 (2014).

47 Burridge, K. & Guilluy, C. Focal adhesions, stress fibers and mechanical tension. *Experimental cell research* **343**, 14-20, doi:10.1016/j.yexcr.2015.10.029 (2016).

48 Gorman, J. L., Ispanovic, E. & Haas, T. L. Regulation of matrix metalloproteinase expression. *Drug Discovery Today: Disease Models* **8**, 5-11, doi:https://doi.org/10.1016/j.ddmod.2011.06.001 (2011).

49 Yang, H. *et al.* Mechanosensitive caveolin-1 activation-induced PI3K/Akt/mTOR signaling pathway promotes breast cancer motility, invadopodia formation and metastasis in vivo. *Oncotarget* **7**, 16227-16247, doi:10.18632/oncotarget.7583 (2016).

50 Ricca, B. L. *et al.* Transient external force induces phenotypic reversion of malignant epithelial structures via nitric oxide signaling. *eLife* **7**, e26161, doi:10.7554/eLife.26161 (2018).

51 Pardo-Pastor, C. *et al.* Piezo2 channel regulates RhoA and actin cytoskeleton to promote cell mechanobiological responses. *Proceedings of the National Academy of Sciences*, doi:10.1073/pnas.1718177115 (2018).

52 Su, S. *et al.* Genetically encoded calcium indicator illuminates calcium dynamics within primary cilia. *Nature methods* **10**, 10.1038/nmeth.2647, doi:10.1038/nmeth.2647 (2013).

53 Srivastava, N., Kay, R. R. & Kabla, A. J. Method to study cell migration under uniaxial compression. *Molecular biology of the cell* **28**, 809-816, doi:10.1091/mbc.E16-08-0575 (2017).

54 Bravo-Cordero, Jose J. *et al.* A novel spatiotemporal RhoC activation pathway locally regulates cofilin activity at invadopodia. *Current Biology* **21**, 635-644, doi:https://doi.org/10.1016/j.cub.2011.03.039 (2011).

55 Oser, M. *et al.* Specific tyrosine phosphorylation sites on cortactin regulate Nck1-dependent actin polymerization in invadopodia. *Journal of cell science* **123**, 3662-3673, doi:10.1242/jcs.068163 (2010).

56 Artym, V. V., Yamada, K. M. & Mueller, S. C. in *Extracellular Matrix Protocols: Second Edition* (eds Sharona Even-Ram & Vira Artym) 211-219 (Humana Press, 2009).

57 Kumar, S., Das, A., Barai, A. & Sen, S. MMP secretion rate and inter-invadopodia spacing collectively govern cancer invasiveness. *Biophysical Journal* **114**, 650-662, doi:https://doi.org/10.1016/j.bpj.2017.11.3777 (2018).

58 Majumder, S. *et al.* Cell-sized mechanosensitive and biosensing compartment programmed with DNA. *Chemical communications (Cambridge, England)* **53**, 7349-7352, doi:10.1039/c7cc03455e (2017).

59 Schindelin, J. *et al.* Fiji: an open-source platform for biological-image analysis. *Nat Methods* **9**, 676-682, doi:10.1038/nmeth.2019 (2012).

Figure 1

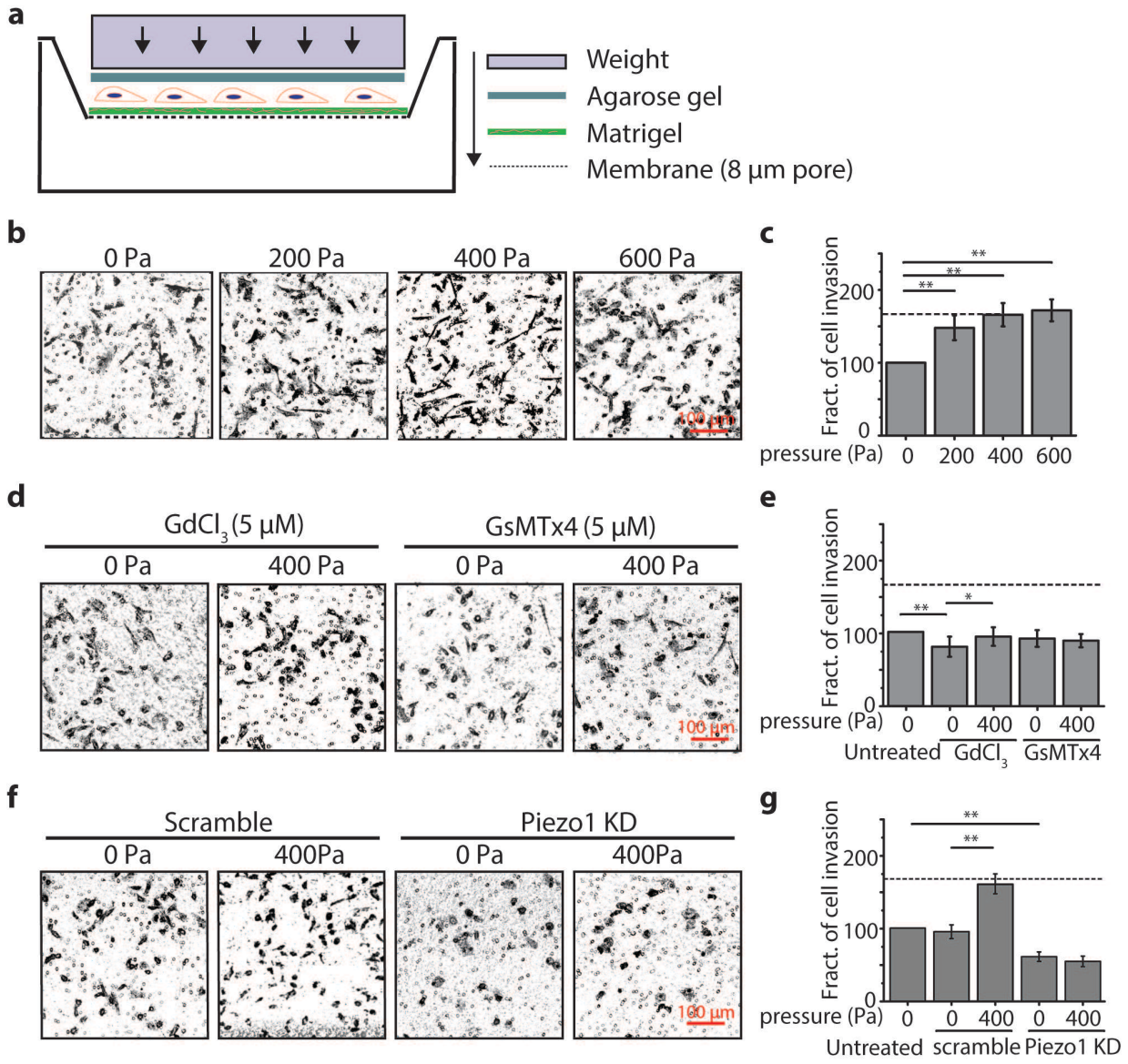
a
Weight
Agarose gel
Matrigel
Membrane (8 µm pore)
b
0 Pa
200 Pa
400 Pa
600 Pa
100 µm
c
Fract. of cell invasion
200
100
0
**
**
**
pressure (Pa) 0 200 400 600
d
GdCl3 (5 µM)
GsMTx4 (5 µM)
0 Pa
400 Pa
0 Pa
400 Pa
100 µm
e
Fract. of cell invasion
200
100
0
**
*
pressure (Pa) 0 0 400 0 400
Untreated GdCl3 GsMTx4
f
Scramble
Piezo1 KD
0 Pa
400Pa
0 Pa
400Pa
100 µm
g
Fract. of cell invasion
200
100
0
**
**
pressure (Pa) 0 0 400 0 400
Untreated scramble Piezo1 KD

Figure 2

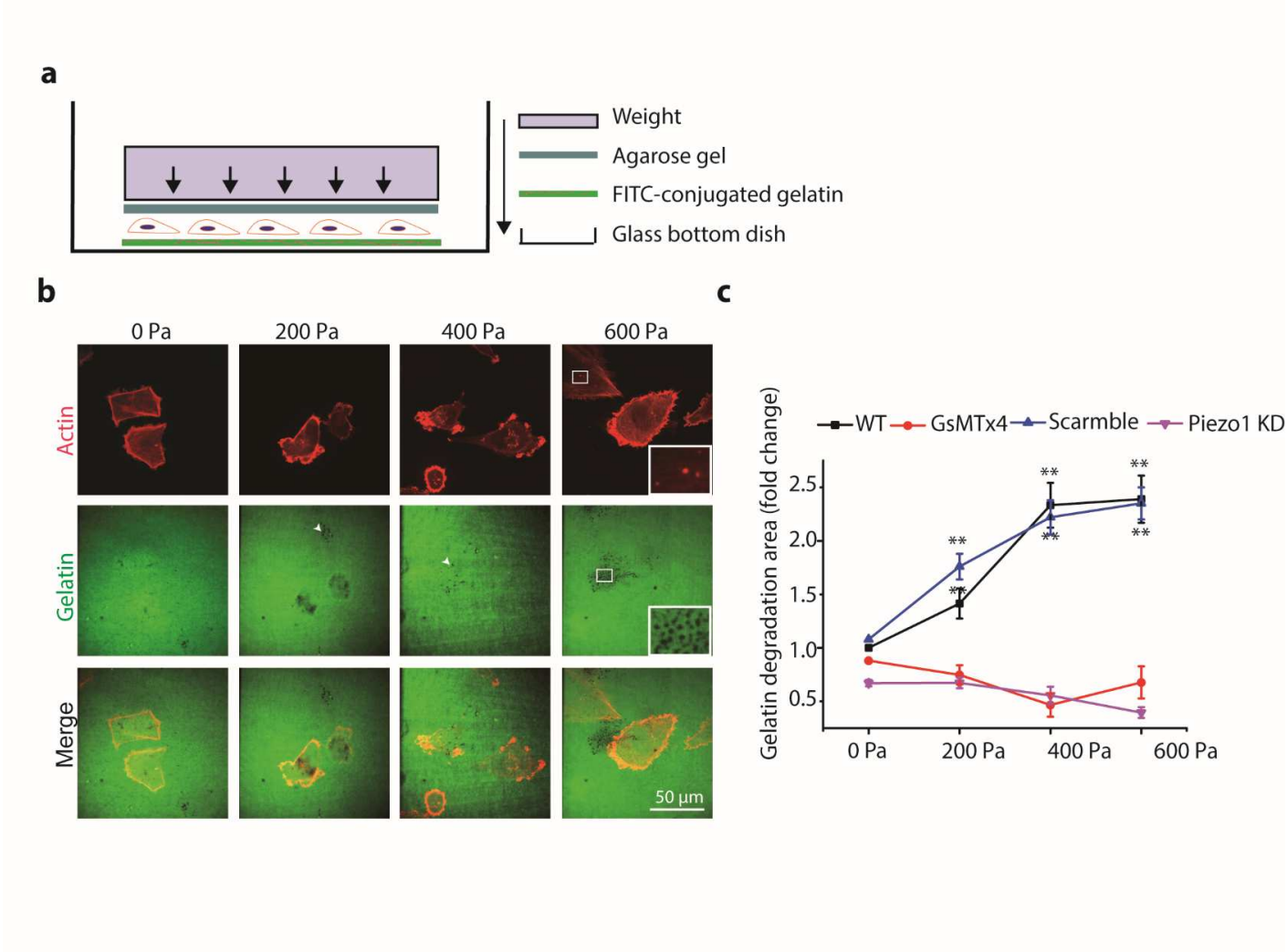
a
Weight
Agarose gel
FITC-conjugated gelatin
Glass bottom dish
b
0 Pa
200 Pa
400 Pa
600 Pa
Actin
Gelatin
Merge
50 μm
c
WT
GsMTx4
Scarmble
Piezo1 KD
Gelatin degradation area (fold change)
2.5
2.0
1.5
1.0
0.5
0 Pa
200 Pa
400 Pa
600 Pa
**

Figure 3

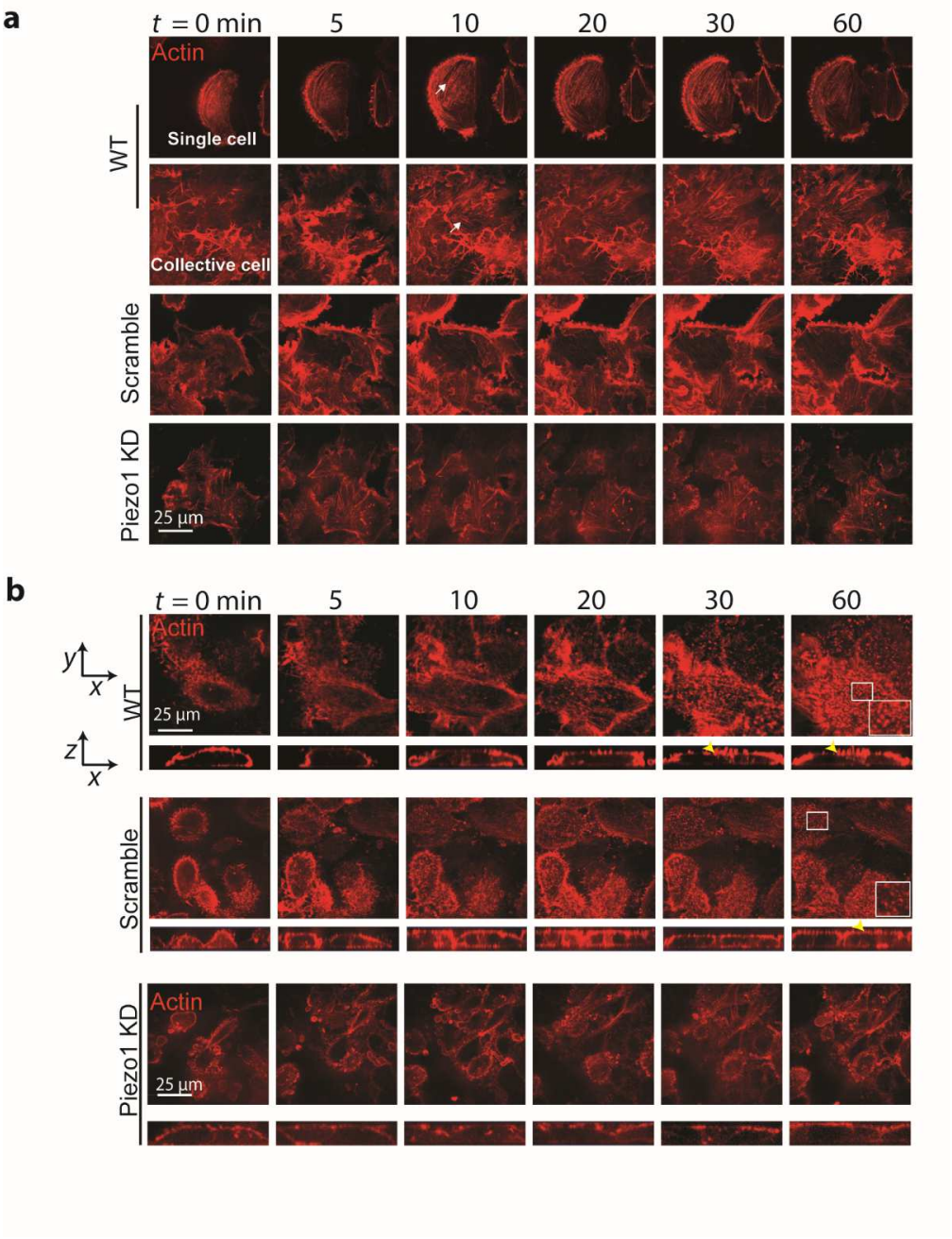
a
t = 0 min
5
10
20
30
60
Actin
Single cell
Collective cell
WT
Scramble
Piezo1 KD
25 μm
b
t = 0 min
5
10
20
30
60
Actin
y
x
z
x
WT
25 μm
Scramble
Actin
Piezo1 KD
25 μm

Figure 4

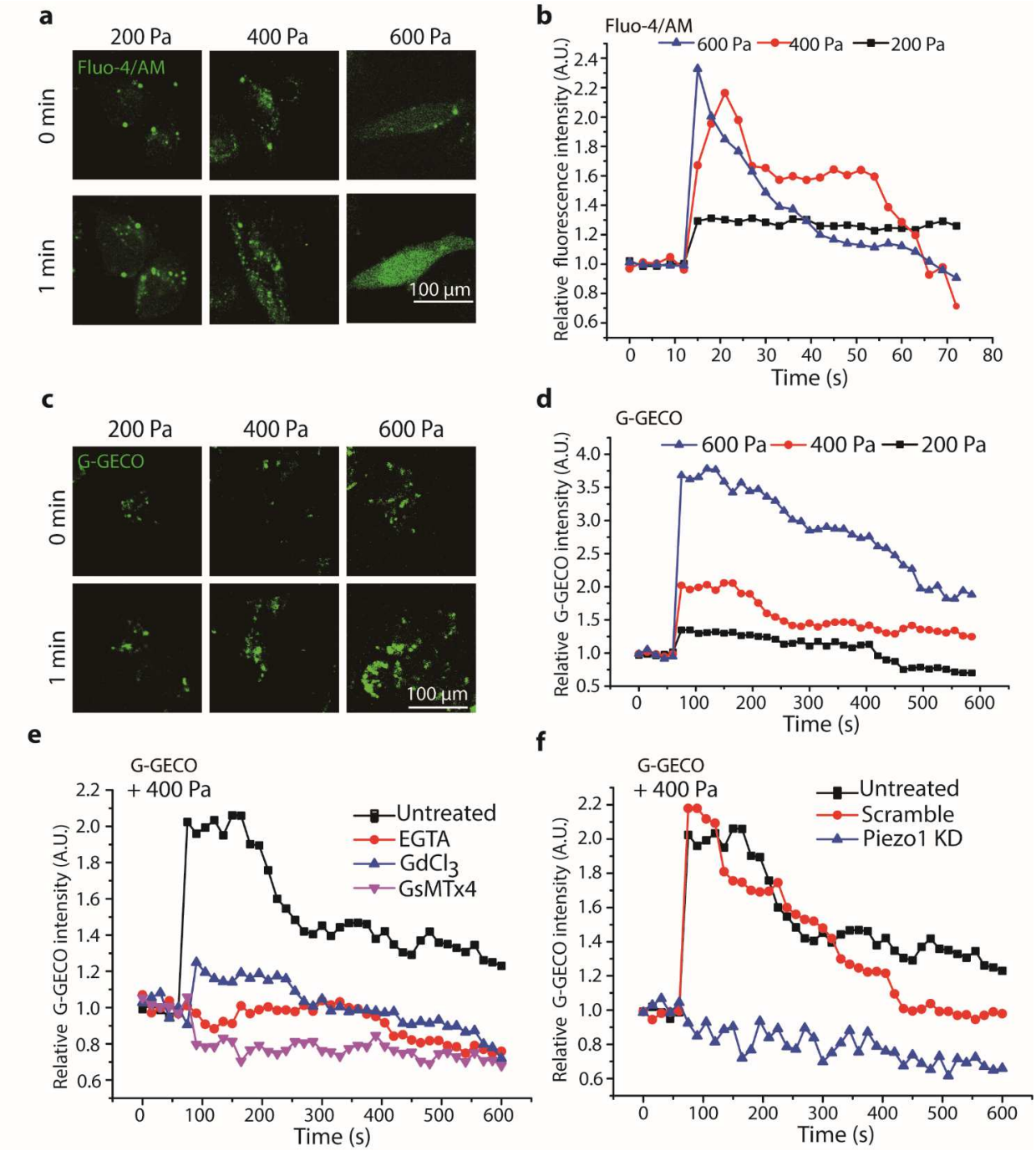
a
200 Pa
400 Pa
600 Pa
Fluo-4/AM
0 min
1 min
100 µm
b
Fluo-4/AM
600 Pa
400 Pa
200 Pa
Relative fluorescence intensity (A.U.)
Time (s)
c
200 Pa
400 Pa
600 Pa
G-GECO
0 min
1 min
100 µm
d
G-GECO
600 Pa
400 Pa
200 Pa
Relative G-GECO intensity (A.U.)
Time (s)
e
G-GECO
+ 400 Pa
Untreated
EGTA
GdCl3
GsMTx4
Relative G-GECO intensity (A.U.)
Time (s)
f
G-GECO
+ 400 Pa
Untreated
Scramble
Piezo1 KD
Relative G-GECO intensity (A.U.)
Time (s)

Figure 5

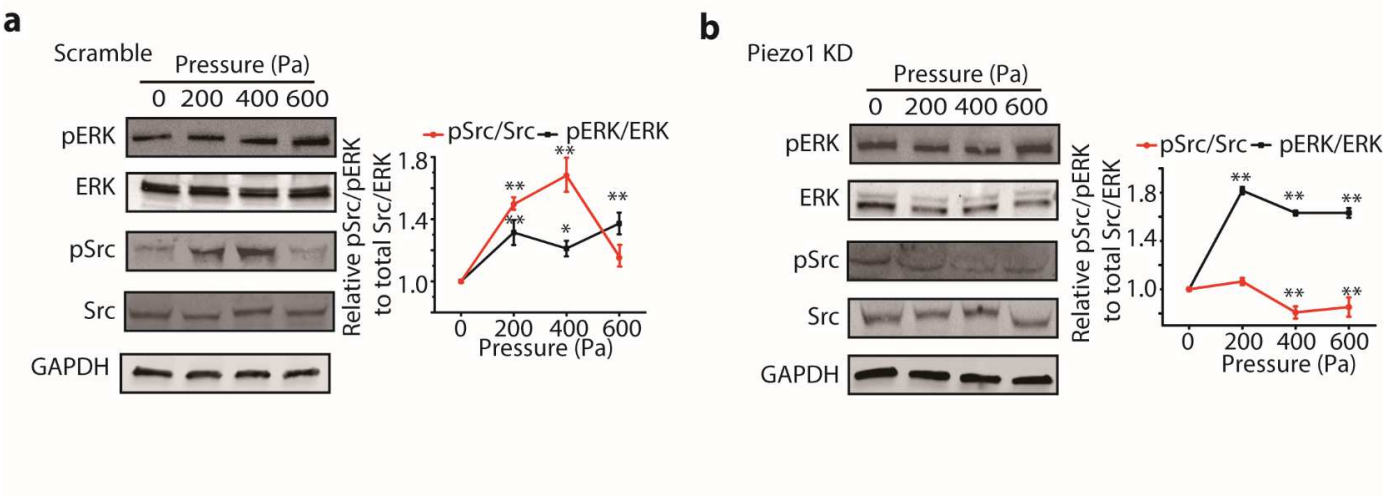
a
Scramble
Pressure (Pa)
0 200 400 600
pERK
ERK
pSrc
Src
GAPDH
pSrc/Src
pERK/ERK
Relative pSrc/pERK to total Src/ERK
1.8
1.4
1.0
0 200 400 600
Pressure (Pa)
b
Piezo1 KD
Pressure (Pa)
0 200 400 600
pERK
ERK
pSrc
Src
GAPDH
pSrc/Src
pERK/ERK
Relative pSrc/pERK to total Src/ERK
1.8
1.4
1.0
0 200 400 600
Pressure (Pa)

Figure 6

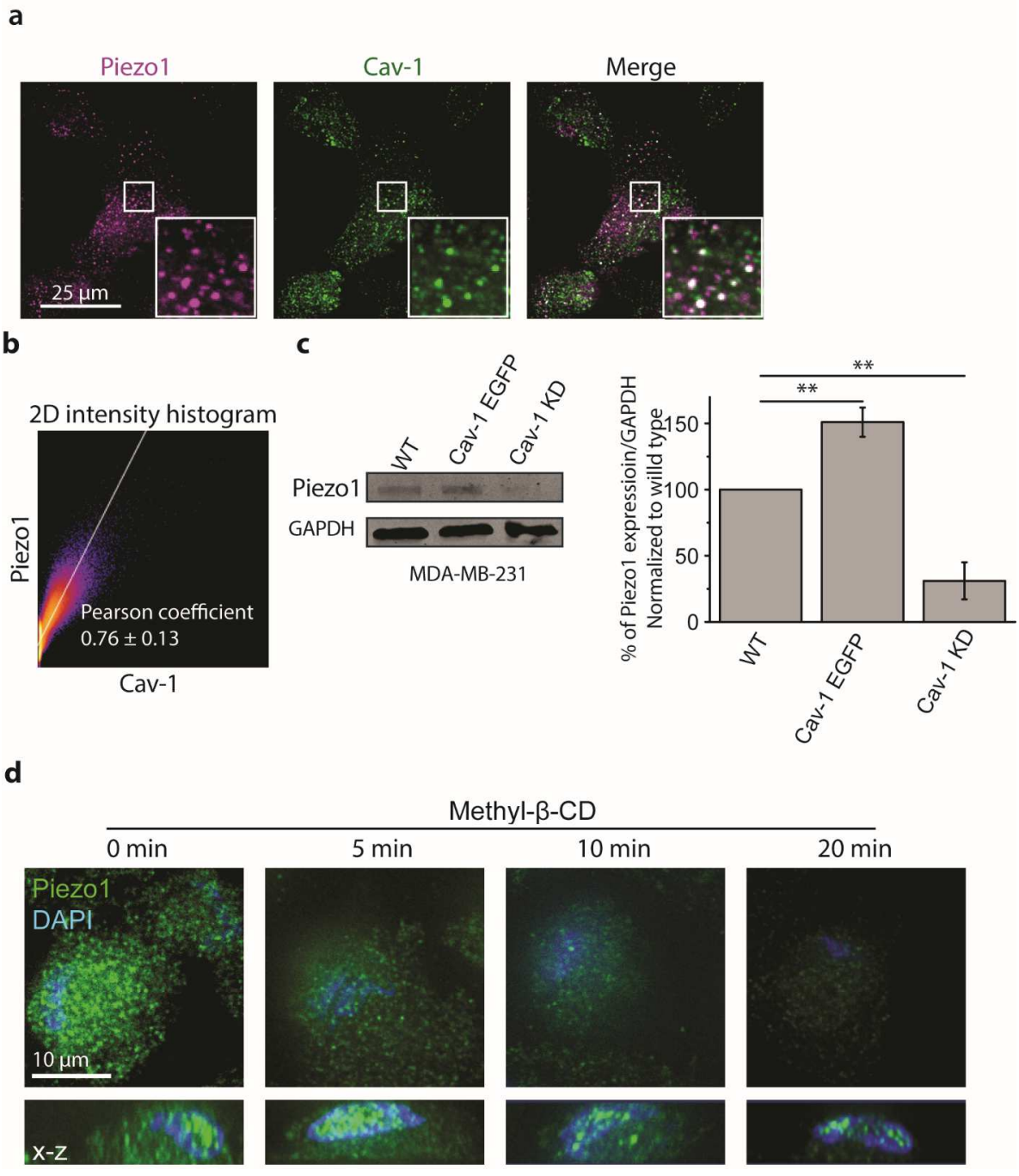
a
Piezo1
Cav-1
Merge
25 μm
b
2D intensity histogram
Piezo1
Pearson coefficient
0.76 ± 0.13
Cav-1
c
WT
Cav-1 EGFP
Cav-1 KD
Piezo1
GAPDH
MDA-MB-231
% of Piezo1 expressioin/GAPDH
Normalized to willd type
150
100
50
0
**
**
WT
Cav-1 EGFP
Cav-1 KD
d
Methyl-β-CD
0 min
5 min
10 min
20 min
Piezo1
DAPI
10 μm
x-z

Figure 7

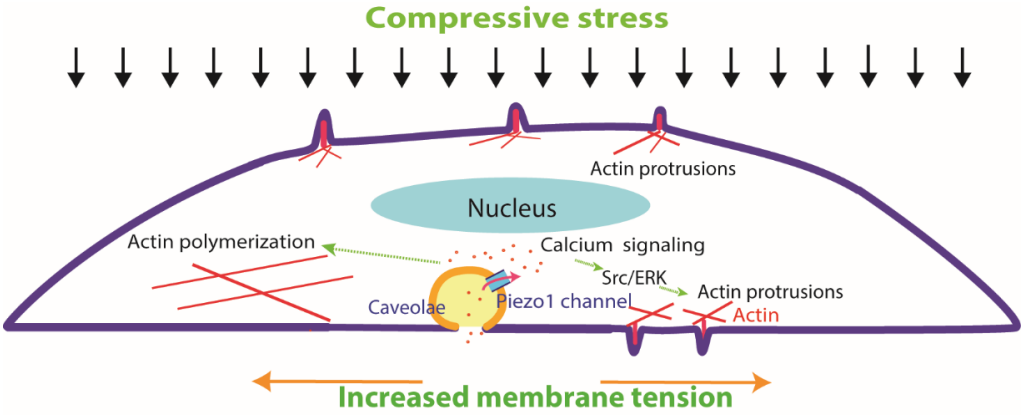
Compressive stress
Actin protrusions
Nucleus
Actin polymerization
Calcium signaling
Src/ERK
Actin protrusions
Caveolae
Piezo1 channel
Actin
Increased membrane tension

Supplemental Information

Compressive Stress Enhances Invasive Phenotype of Breast Cancer Cells via Piezo1 Activation

Mingzhi Luo[1,2], Kenneth K. Y. Ho[1], Zhaowen Tong[3], Linhong Deng[2,*], Allen P. Liu[1,3,4,5,*]

[1] Department of Mechanical Engineering, University of Michigan, Ann Arbor, Michigan, United States

[2] Institute of Biomedical Engineering and Health Sciences, Changzhou University, Changzhou, Jiangsu, P. R. China

[3] Department of Biophysics, University of Michigan, Ann Arbor, Michigan, United States

[4] Department of Biomedical Engineering, University of Michigan, Ann Arbor, Michigan, United States

[5] Cellular and Molecular Biology Program, University of Michigan, Ann Arbor, Michigan, United States

* Corresponding author: Linhong Deng, +86-13685207009, dlh@cczu.edu.cn; Allen P. Liu, +1-734-764-7719, allenliu@umich.edu

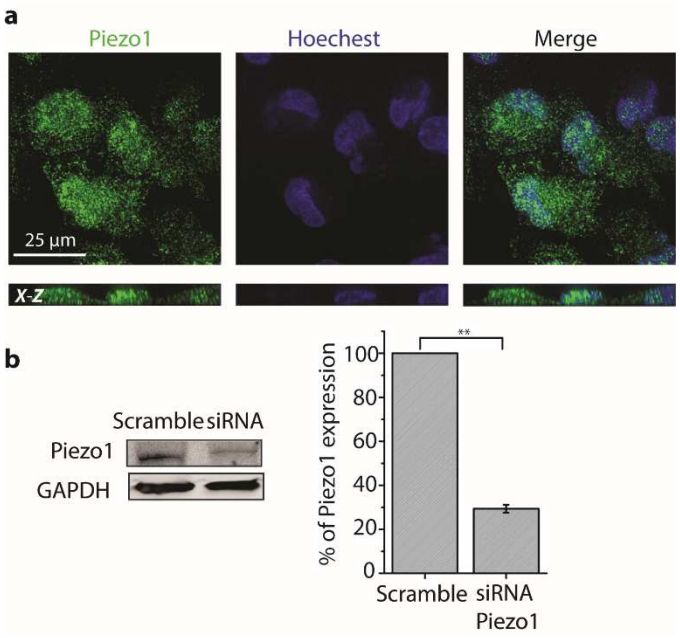

Figure S1 The distribution and the efficiency of siRNA knockdown (KD) of Piezo1 in MDA-MB-231 breast cancer cells. **a** Representative confocal microscopy images of immunostained Piezo1 in MDA-MB-231 cells (100X). Piezo1 (green) and nucleus (blue) were detected with antibodies and Hoechest 33342, respectively, showing puncta structures of Piezo1 localized in plasma membrane, cytosol, and nucleus. **b** Efficiency of siRNA KD for Piezo1. The cells were transfected with scramble control or siRNA probes for Piezo1 for 48 h and Piezo1 expression was determined by Western blot. The bar graphs show the percentage of Piezo1 in scramble and siRNA groups (** p <0.01, n = 3).

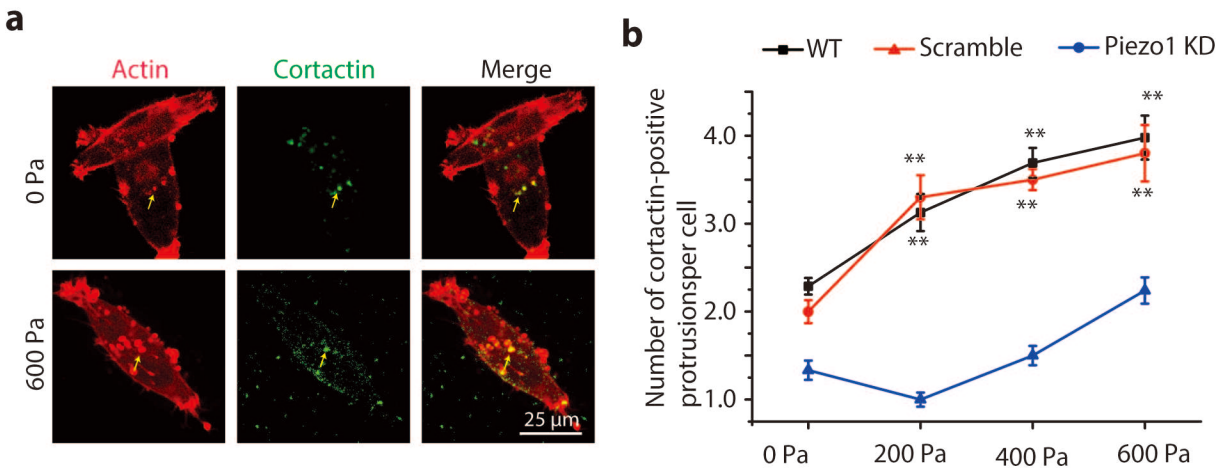

Figure S2 a Representative images (red: actin, green: cortactin) of invadopodia (yellow arrows) in MDA-MB-231 cells with or without 600 Pa compression. Control and compressive stress-treated MDA-MB-231 cells were cultured on gelatin-coated glass bottom dish for 8 h, then fixed and stained with phalloidin to visualize F-actin (red) and antibody for cortactin (green). **b** The average number (± SD) of basal cortactin-positive actin puncta per cell under compression with or without Piezo1 KD. n = 20 - 30.

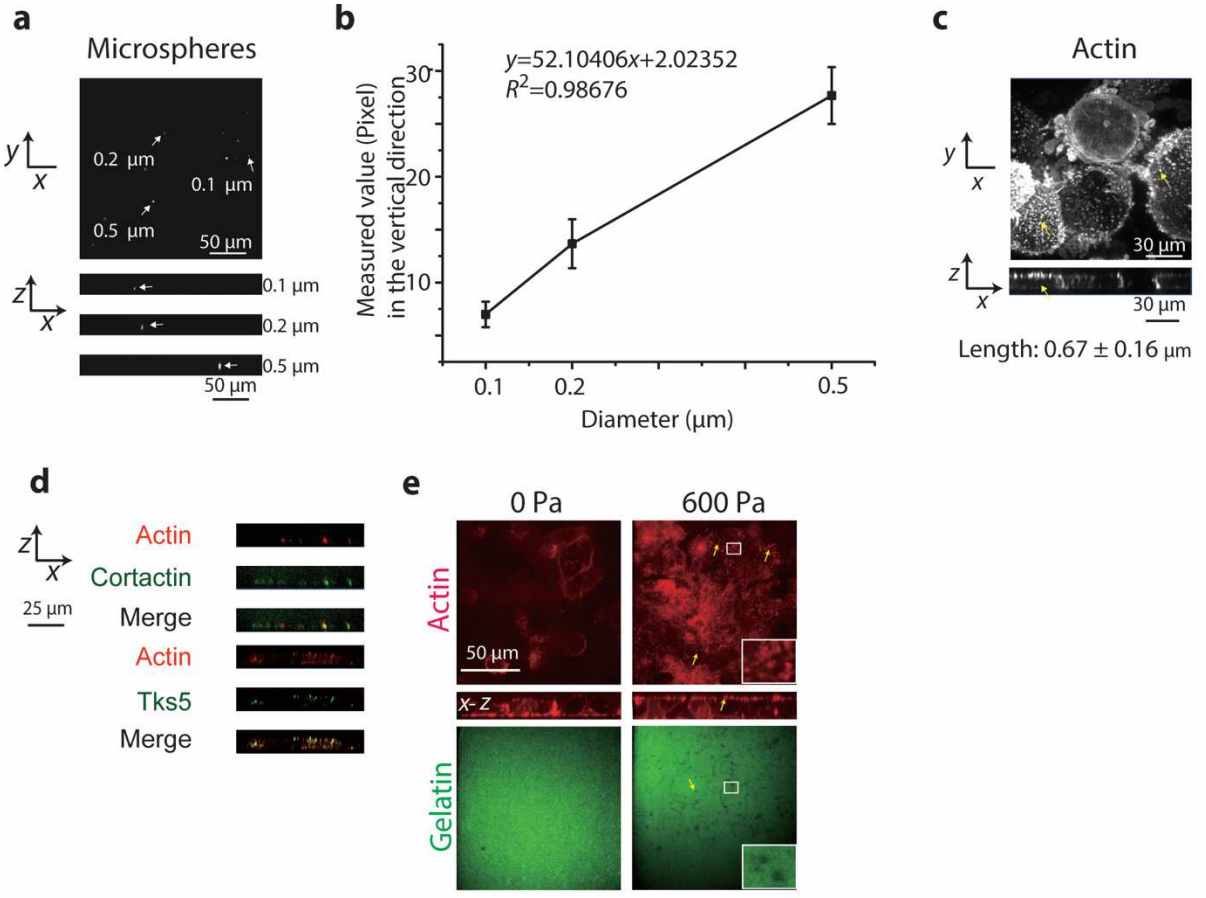

Figure S3 The characterization of upward actin protrusion. **a** Representative confocal microscopic images (100X) of microspheres (diameter = 0.1 μm, 0.2 μm or 0.5 μm, respectively). **b** The linear relationship between the measured value (pixel ± SD) in the vertical direction and the diameter of the microspheres. **c** Representative confocal microscopic images (100X) of apical actin protrusions. **d** Representative images (60X) of immunostained cortactin and Tks5 with actin protrusion in MDA-MB-231 cells expressing Lifeact-RFP under compression (600 Pa) for 60 min. **e** Representative images of actin protrusions at the apical side of cells that degraded gelatin. Insets of 600 Pa images are magnified view of the boxed regions.

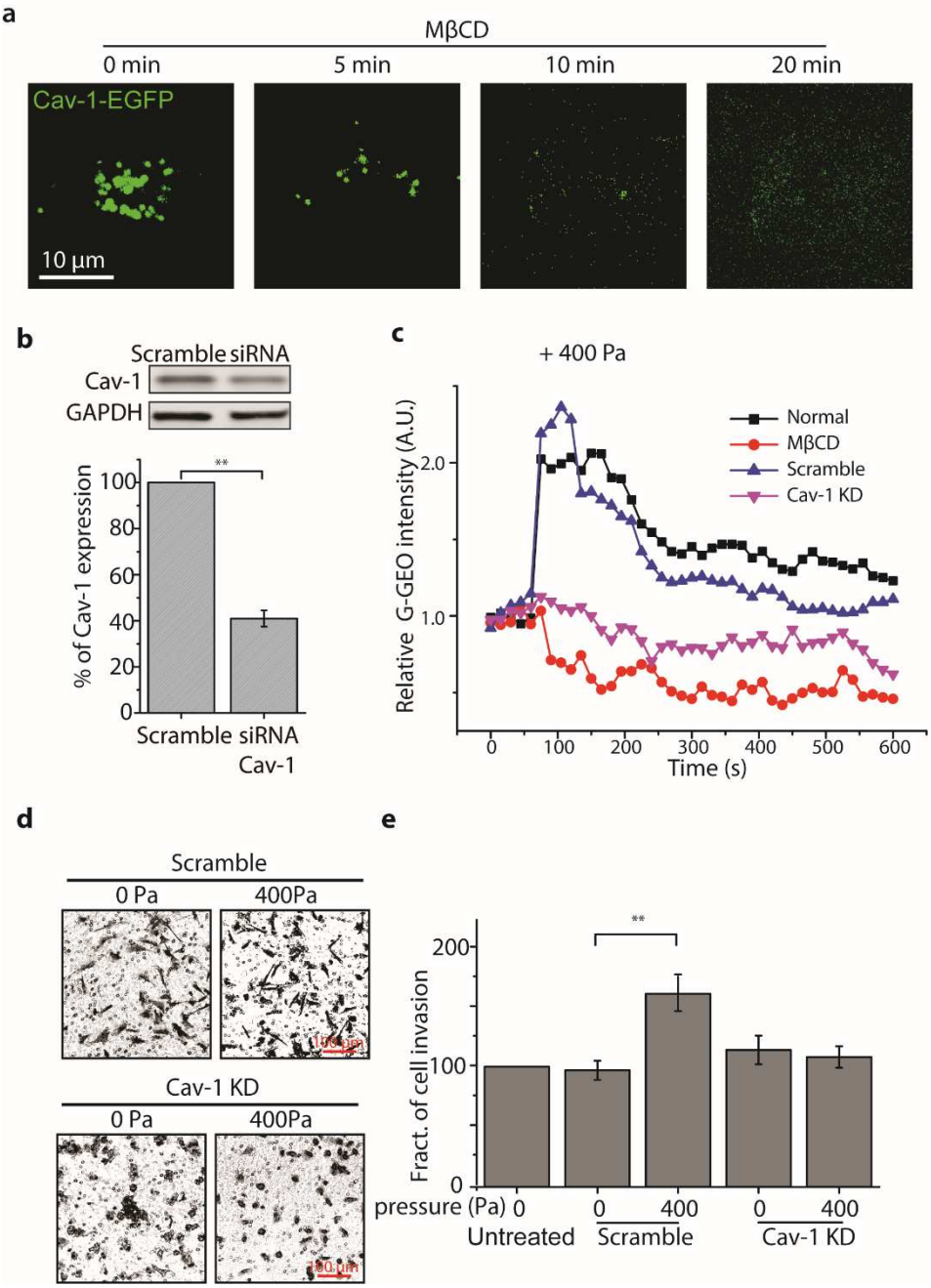

Figure S4 Caveolae regulate the function of Piezo1 in responding to compressive stress in MDA-MB-231 cells. **a** Effect of methyl-beta-cyclodextrin (MβCD) on removing caveolae from the plasma membrane. Cells expressing Cav-1-EGFP were treated with 5 mM of MβCD for 5 min, 10 min, and 20 min at 37 °C and imaged by spinning disk confocal microscopy (100X). The representative images show that MβCD dramatically removed caveolae from the plasma membrane within 20

min of the drug administration. **b** Efficiency of siRNA knockdown (KD) for caveolin1 (Cav-1). The cells were transfected with scramble control or siRNA probes for Piezo1 for 48 h and Piezo1 expression was determined by Western blot. The bar graphs show the percentage of Piezo1 in scramble and siRNA groups (** $p < 0.01$, n = 3). **c** Average time-courses of relative mean fluorescence intensity of G-GECO in MDA-MB-231 cells pretreated with or without MβCD, and Cav-1 KD in response to 400 Pa compressive stress. Each experiment assayed 10-20 cells and repeated three times. **d, e** Representative images of invaded cells and quantification of percentage of invaded cells treated with siRNA for Cav-1 under 400 Pa.

Video 1 Representative video recording the real time intracellular [Ca^{2+}] response of MDA-MB-231 labeled with Fluo-4/AM before (0 min) and after (1 min) exposure to 400 Pa compressive stress**.**

Video 2 Representative video recording the real time intracellular [Ca^{2+}] response of MDA-MB-231 transiently expressing G-GECO before (0 min) and after (1 min) exposure to 400 Pa compressive stress**.**

Figures

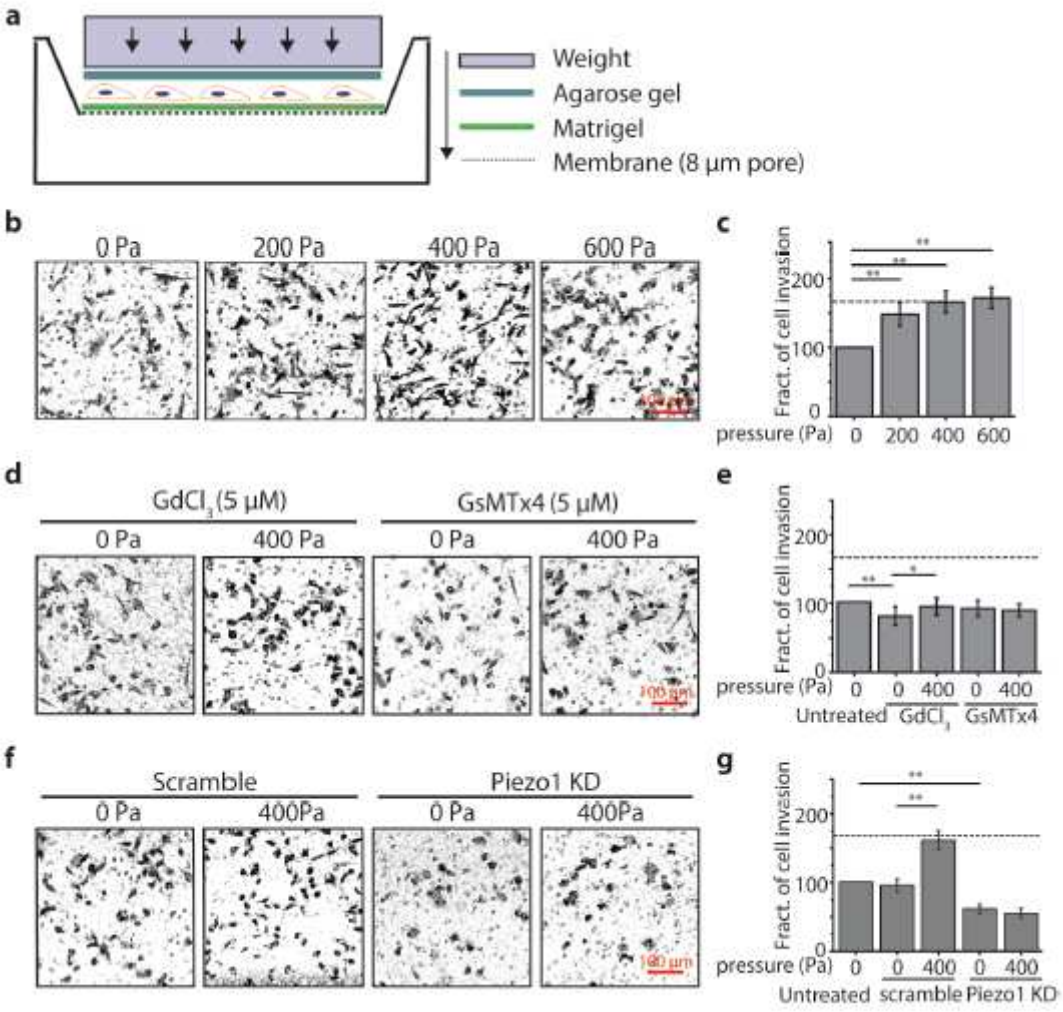

Figure 1

Compressive stress enhanced invasion of MDA-MB-231 cells depending on Piezo1. Cell invasion was measured with in vitro transwell invasion assay. a Schematic diagram of the compression experiment using a transwell setup. Cells grown on membrane filter (8 μm pore) coated with Matrigel for 6 h were covered with 1% of agarose gel and compressed with a specific weight. b, c Representative images of invaded cells stained with crystal violet under different compressive stress and quantification of percentage of invaded cells. d, e Representative images of invaded cells and quantification of percentage of invaded cells treated with Gadolinium chloride (Gd3+) or GsMTx4 under 400 Pa. f, g Representative images of invaded cells and quantification of percentage of invaded cells treated with siRNA for Piezo1 under 400 Pa. Dashlines in c indicate cell invasion under 400 Pa without any perturbations, n = 3. *p < 0.05 versus control groups; ** p < 0.01 versus control groups. Error bars represent s.e.m..

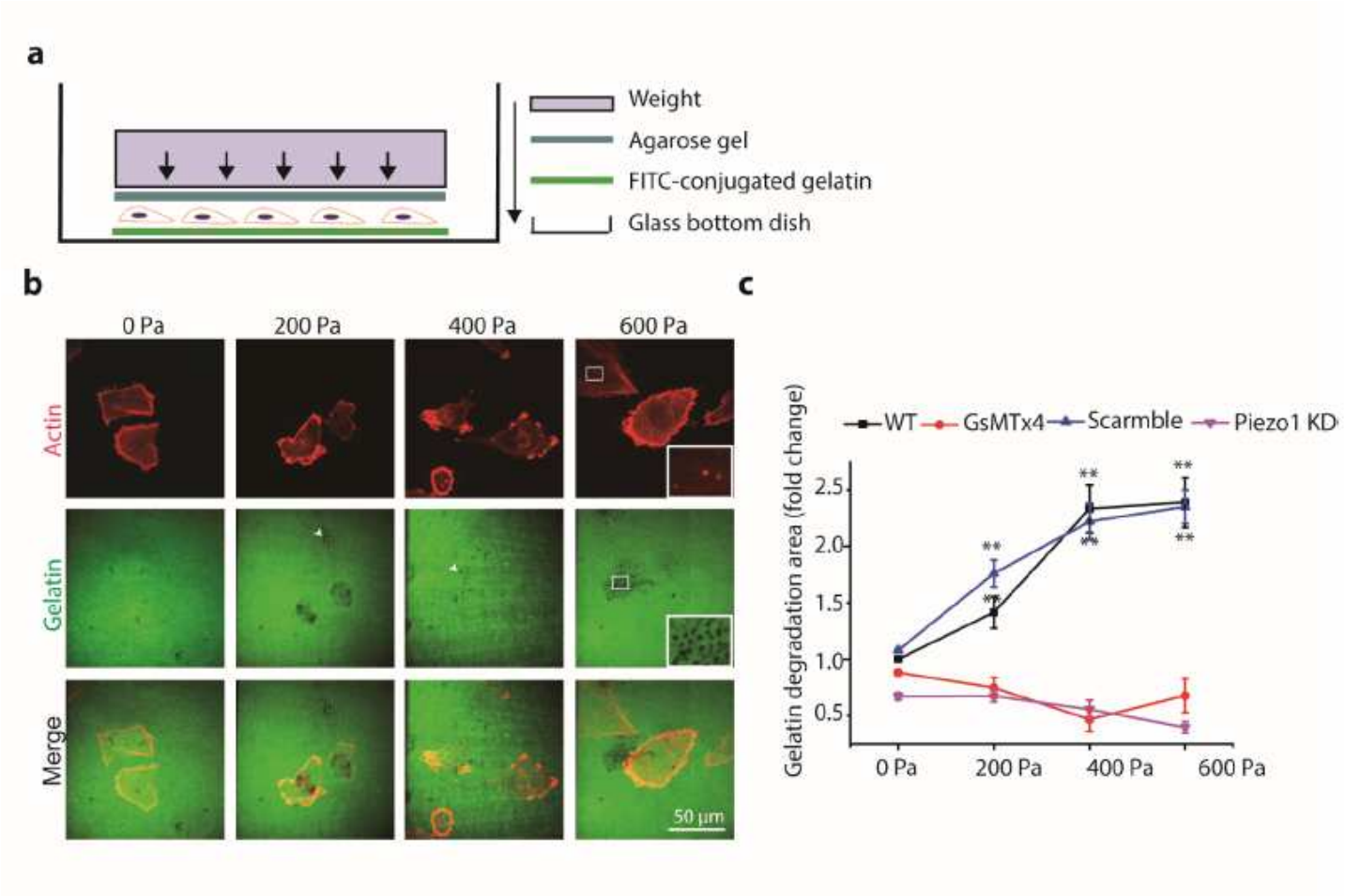

Figure 2

Compressive stress promoted matrix degradation in MDA-MB-231 cells. a Schematic diagram of the experiment. Cells grown on a glass-bottom dish coated with FITC-conjugated gelatin for 8 h were covered with 1% of agarose gel and compressed with a specific weight. b Representative images (red: actin, green: gelatin) of compression-promoted gelatin degradation at the ventral side of the cell. Gelatin degradation was visualized by confocal microscopy as disappearance of green fluorescence. The arrow in 200 Pa shows an example of the punctate gelatin-degraded region. Insets of 600 Pa images are magnified view of the boxed regions. c The fold change of gelatin degradation area under different treatment conditions as a function of compressive stress normalized to gelatin degradation area at 0 Pa. ** $p < 0.01$ versus control groups. Error bars represent s.e.m..

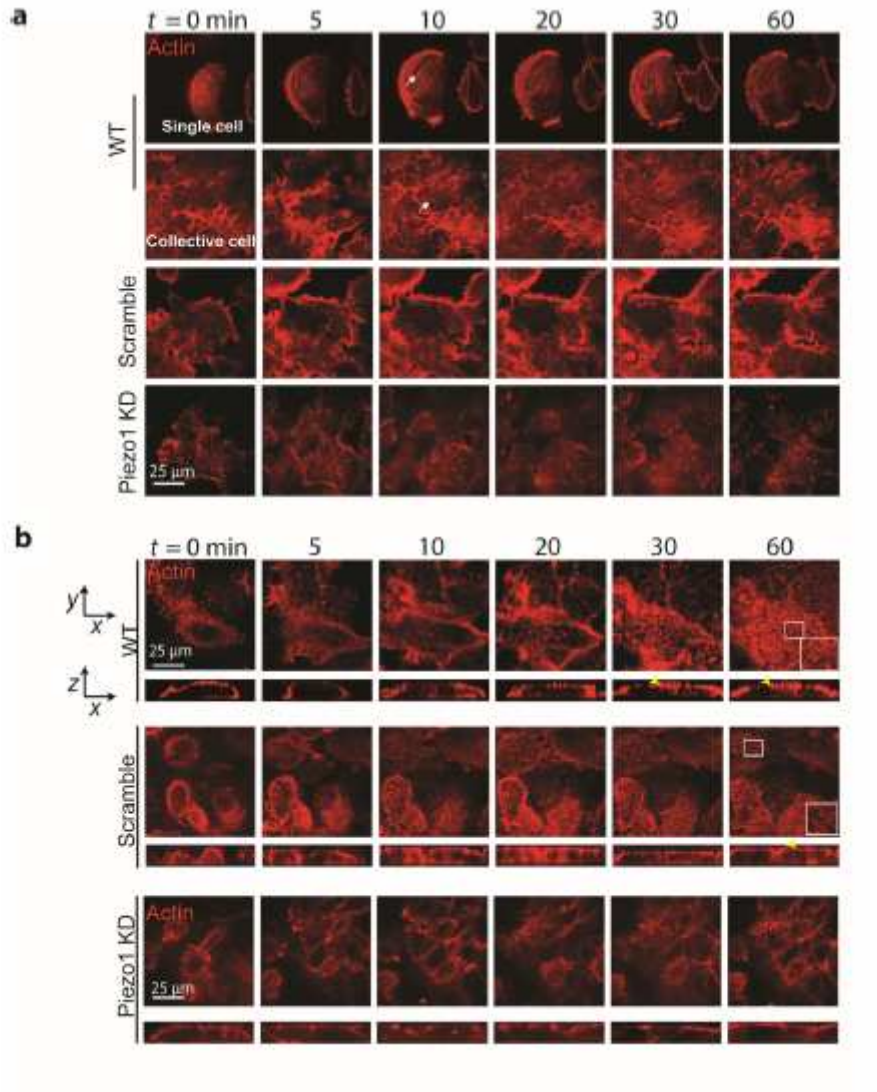

Figure 3

Piezo1 mediated compressive stress-induced formation of stress fiber and actin protrusions. a Representative images of stress fiber at the ventral side of MDA-MB-231 cells expressing Lifeact-RFP with (600 Pa, bottom panel) or without Piezo KD under compression (600 Pa, upper panel with single cell or collective cells) for 60 min (white arrows in the images show the stress fiber formation). b Representative images of actin protrusions at the apical side of MDA-MB-231 cells expressing Lifeact-RFP under compression (600 Pa) for 60 min (see magnified views and yellow arrow heads in the images at 30 and 60 min).

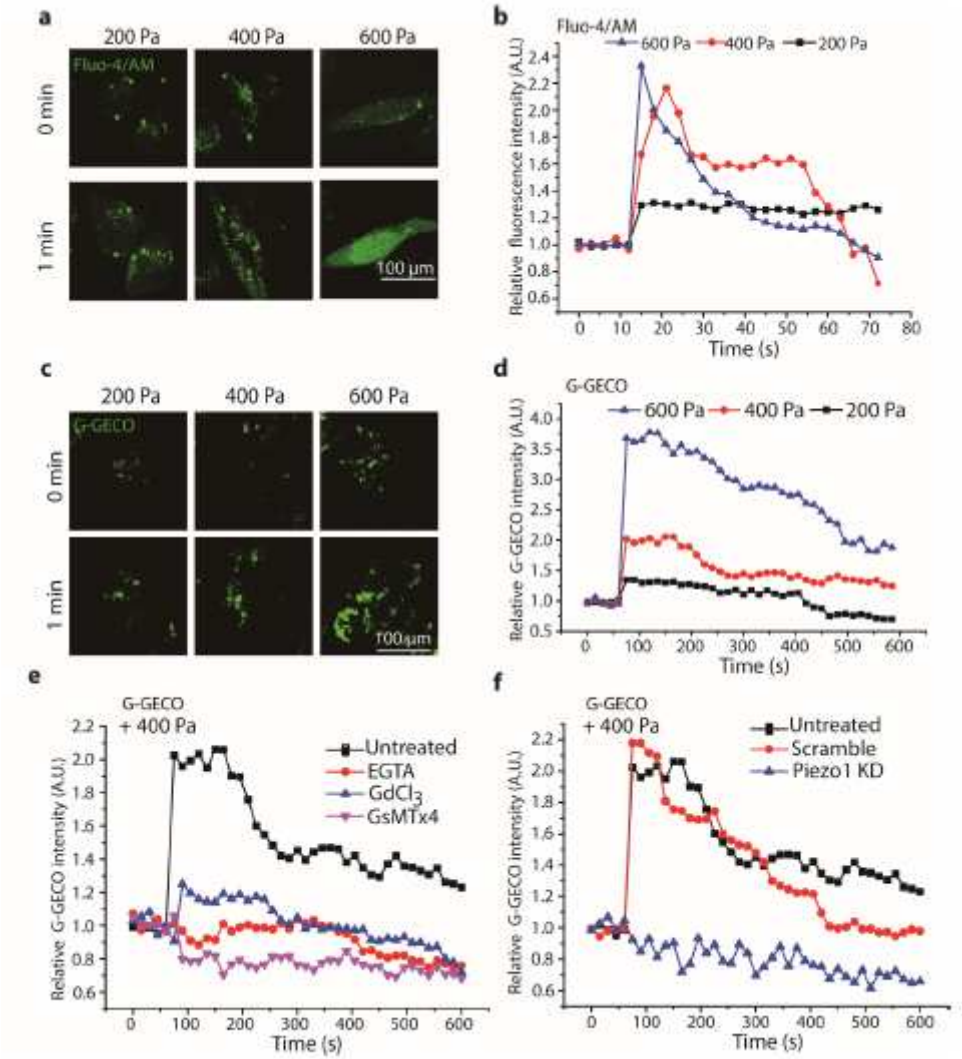

Figure 4

Compressive stress induced calcium signaling in MDA-MB-231 cells. Representative images of intracellular [Ca2+] (a and c) and average time-courses of changing relative mean fluorescence intensity (b and d) of Fluo-4 or G-GECO (normalized to time 0) in MDA-MB-231 cells labeled with Fluo-4/AM or transiently expressing G-GECO before (0 min) and after (1 min) exposure to compressive stress at 200, 400, 600 Pa, respectively. e, f Time-courses of changing relative mean fluorescence intensity of G-GECO in MDA-MB-231 cells pretreated with or without EGTA, Gd3+, GsMTx4, and Piezo1 KD in response to 400 Pa compressive stress. Each experiment assayed 10-20 cells and repeated three times.

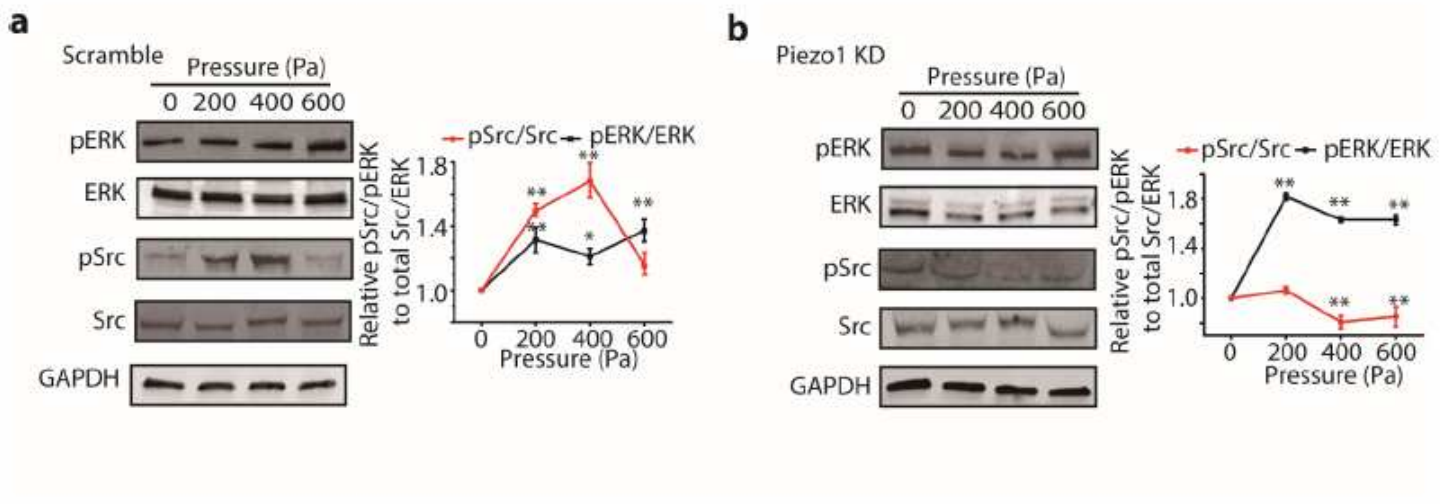

Figure 5

Compression enhanced the activity of ERK and Src. a The phosphorylation of ERK and Src in MDA-MB-231 cells pretreated with scramble probes in the absence or presence of compressive stress at 200, 400, 600 Pa. b The phosphorylation of ERK and Src in MDA-MB-231 cells pretreated with siRNA for Piezo1 in the absence or presence of compressive stress at 200, 400, 600 Pa. Relative phosphorylation levels were obtained by normalizing to GAPDH expression and 0 Pa value, n = 3. *p < 0.05 versus control groups; ** p < 0.01 versus control groups. Error bars represent s.e.m..

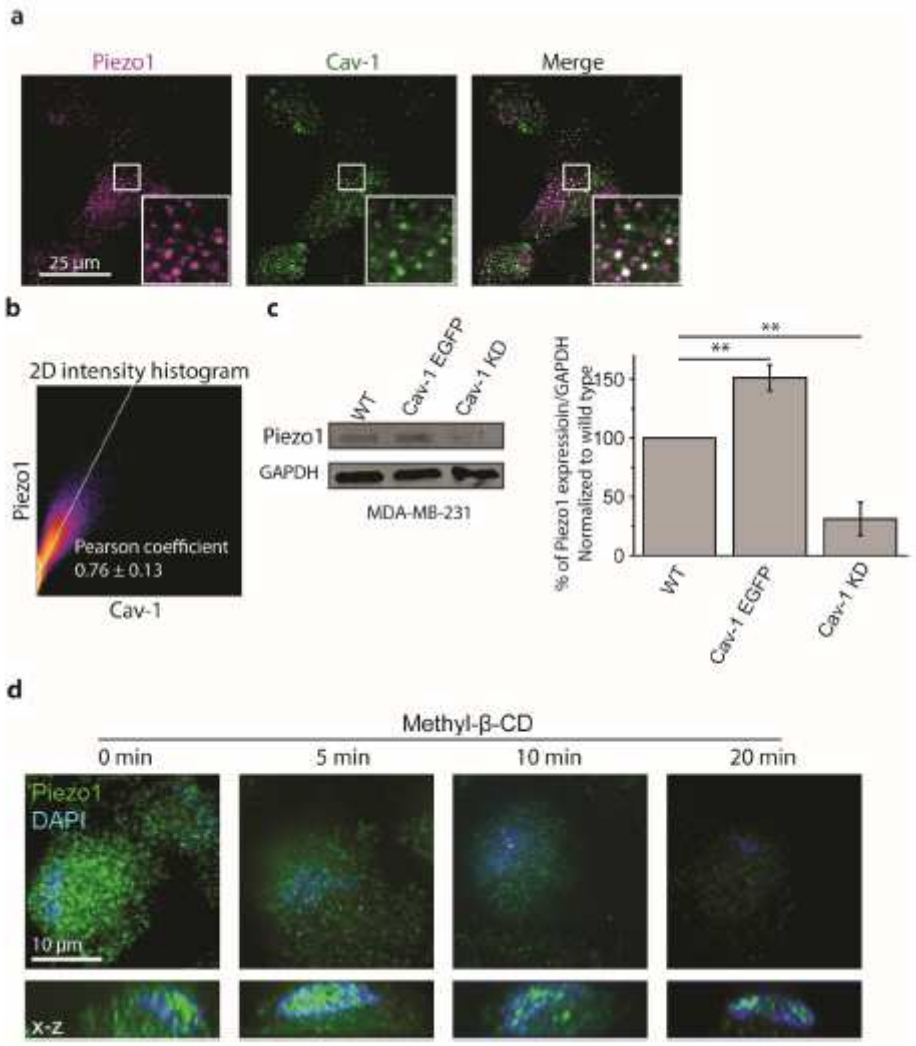

Figure 6

The expression and distribution of Piezo1 in MDA-MB-231 cells were regulated by caveolae. a Representative fluorescence images of Piezo1 (magenta) and caveolae (green) colocalization and 2D intensity histogram output in MDA-MB-231 cells. Insets in both conditions show magnified view of the boxed regions. b Representative image of 2D intensity histogram output of Coloc2 analysis performed using Fiji software. The text indicates the Pearson coefficient (± SD) of the pixel-intensity correlation (n = 8). c Western blot images and quantification of Piezo1 expression in wield type (WT), Cav-1 EGFP expressing, and Cav-1 KD MDA-MB-231 cells (n = 3). *p < 0.05 versus control groups; ** p < 0.01 versus control groups. d, Representative fluorescence images of Piezo1 (green) and nucleus (blue) after cells were treated with MβCD for 5 min, 10 min, and 20 min (upper panel: x-y view, lower panel: x-z view). Error bars represent s.e.m..

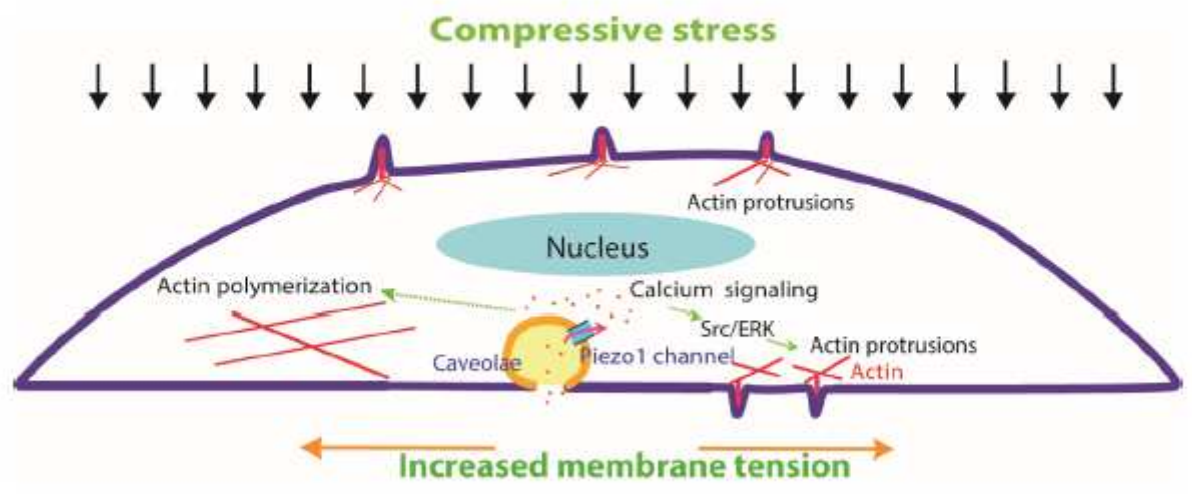

Figure 7

Model of compressive stress-promoted invasive phenotype of MDA-MB-231 cells and associated signaling pathways. Together, vertical mechanical compressive stress increases the lateral plasma membrane tension and activates Piezo1 channels. The opening of Piezo1 mediates the influx of calcium and evokes downstream signaling pathways such as Src. These activated signaling molecules promote actin protrusions both at the apical and ventral sides of cells and the remodeling of actin cytoskeleton, which in turn mediate enhanced matrix degradation and cell invasion.

Supplementary Files

This is a list of supplementary files associated with this preprint. Click to download.

- Video1.avi
- Video2.avi